

Final Report  
Project A-1642

7-2-87

7-83

## RESEARCH IN MILLIMETER WAVE TECHNIQUES

By

R. W. McMillan

Prepared for

National Aeronautics and Space Administration  
Goddard Space Flight Center  
Greenbelt, Maryland 20771

Under

NASA Grant NSG-5012

June 17, 1987

**GEORGIA INSTITUTE OF TECHNOLOGY**  
A Unit of the University System of Georgia  
Atlanta, Georgia 30332



1987



**RESEARCH IN MILLIMETER WAVE  
TECHNIQUES**

**Final Report on Project A-1642**

**by  
R. W. McMillan**

**Georgia Institute of Technology  
Georgia Tech Research Institute  
Atlanta, Georgia 30332**

**Prepared for**

**National Aeronautics and Space Administration  
Goddard Space Flight Center  
Greenbelt, Maryland 20771**

**NASA Grant NSG-5012**

**June 17, 1987**

## Table of Contents

Section	Title	Page
	List of Figures	iii
	Abstract	vi
1.	Introduction	1
1.1	Background	1
1.2	Summary of Areas of Investigation	1
2.	Calculations of Atmospheric Attenuation and Radiometric Antenna Temperature	4
3.	Results of Calculations and Measurements of MMW Attenuation Coefficients and Radiometric Antenna Temperatures	13
3.1	Calculations	13
3.2	Measurements	21
3.2.1	Attenuation Measurements	21
3.2.2	Radiometric Measurements	26
4.	Mixer Research	34
4.1	Single-Ended Mixers	35
4.1.1	Sharpless Wafer Mixers	38
4.1.2	Split-Block Mixer	40
4.1.3	Diplexers for Single-Ended Mixers	42
4.1.4	Local Oscillator Doublers for Single-Ended, Fundamental Mixers	48
4.2	Subharmonic Mixers	48

## Table of Contents

Section	Title	Page
5.	Properties of Wire Grid Arrays	58
5.1	Calculations of Transmission and Reflection	58
5.2	Measurements and Calculations of the Properties of Wire Grid Arrays	64
6.0	Summary and Conclusions	69
	References	72
	Acknowledgements	71

**List of Figures**

Page

Figure 2-1.	Water vapor density vs. altitude measured by radiosonde at Kennedy Airport, and used for zenith attenuation calculations at 230 GHz.	8
Figure 2-2.	Atmospheric temperature profile at Kennedy Airport used for zenith attenuation calculation at 230 GHz.	9
Figure 3-1.	Calculated horizontal atmospheric attenuation due to water vapor as a function of frequency.	14
Figure 3-2.	Calculated total zenith attenuation from sea level for the range 150-700 GHz under the same conditions as used for Figure 3-1.	16
Figure 3-3.	Calculated zenith antenna temperature in the range 150-700 GHz under the same conditions as used for Figure 3-1.	17
Figure 3-4.	Calculated clear-air zenith antenna temperature viewing the sun as a source.	19
Figure 3-5.	Calculated antenna temperature looking down from 50 km. The conditions are indicated on the figure.	20
Figure 3-6.	Calculated antenna temperature due to the 183 GHz water vapor transition viewed looking downward from 50 km. The numbers correspond to the different profiles of Figure 3-7.	22
Figure 3-7.	Atmospheric water vapor distributions used for the calculations shown in Figure 3-6. The numbers of the distributions correspond to the numbers on the curves of Figure 3-6.	23
Figure 3-8.	Diagram of MMW propagation link.	24
Figure 3-9.	Photograph of transmitter end of propagation link. The antenna was housed in a teflon box for all-weather operation.	25
Figure 3-10.	Block diagram of 183 GHz radiometer.	27
Figure 3-11.	Results of measuring the antenna temperature near the 183 GHz water vapor transition on a hot, humid summer day. Calculated values using various models are shown for comparison.	29

**List of Figures****Page**

Figure 3-12.	Comparison of calculated zenith attenuation using various lineshapes to measured results. The dashed line represents the empirical relation $A(\text{dB}) = 0.35 \rho (\text{g/m}^3)$ .	30
Figure 3-13.	Diagram of radiometric load developed with support from this grant.	33
Figure 4-1.	Scanning electron microscope photograph of whisker contacting a GaAs chip to form a diode. Note the array of holes as described in the text. The line at the lower left is a reference distance of 4 microns.	36
Figure 4-2.	Scanning electron microscope photograph of a faulty diode contact showing a damaged whisker. The line at the lower left is a reference distance of 1 micron.	37
Figure 4-3.	Sketch of a sharpless wafer diode mount.	39
Figure 4-4.	Diagram of the split-block single-ended 183 GHz mixer used for early Convair 990 flights as described in the text.	41
Figure 4-5.	A resonant cavity coupler used for diplexing signal and LO.	44
Figure 4-6.	Schematic diagram of the Gustincic diplexer made of two pairs of wire grids forming an interferometer.	46
Figure 4-7.	Photograph of the 91.5/183 GHz doubler designed and built by AIL for this project.	49
Figure 4-8.	Schematic diagram of the subharmonic mixer designed and built with support from this grant. Both f/2 and f/4 versions of this mixer were built.	51
Figure 4-9.	Photograph of assembled f/2 subharmonic mixer. The signal port is at top, the LO port is below, and the IF output is to the right.	54

**List of Figures**

**Page**

Figure 4-10.	Photograph of f/2 mixer disassembled to show stripline channel immediately below IF port.	55
Figure 4-11.	Scanning electron microscope photograph of diode and whisker mounted to stripline. A diode and a whisker are pushed up from below to contact the mixer as shown.	56
Figure 5-1.	Diagram showing the conventions chosen for orientation of grid wires.	59
Figure 5-2.	Comparison of calculated (solid line) and measured (circles) transmission of a four-grid array at 70 GHz. The angle between the grid wires was chosen to be 85°.	65
Figure 5-3.	Calculated values of four-grid array transmission as a function of frequency for three different angles between grid pairs.	66
Figure 5-4.	Four-grid array transmission vs. frequency, showing bandpass and band reject frequencies.	67

## ABSTRACT

This report describes work done at Georgia Tech on NASA grant NSG-5012 "Research in Millimeter Wave Techniques" during the period June 1974 to September, 1986. The objective of this program was to benefit the area of millimeter wave (MMW) technology, with emphasis on the needs of NASA in this rapidly-developing discipline. These interests are primarily in the area of remote sensing, ultimately from spacecraft but also from aircraft. As will become evident upon reading this report, research done during the term of this grant has also benefited other government agencies, as well as the MMW community in general.

The areas of MMW research emphasized at Georgia Tech with support from NSG-5012 include atmospheric propagation and radiometry, advanced MMW component design with emphasis on quasi-optical techniques, and the development of MMW receivers, especially those using subharmonic mixers. Calculations of atmospheric attenuation and radiometric antenna temperature have been made in the range 100-700 GHz, together with measurements of atmospheric antenna temperature near 95 and 183 GHz. This latter frequency is of interest to NASA because it is used in determining atmospheric water vapor profiles. Quasi-optical components designed with grant support include lenses, mirrors, and wire grid devices, as well as feed horns for interface with waveguide components. Subharmonic mixers with state-of-the-art performance at 183 GHz have also been developed, and spin-offs from this technology have benefited other NASA programs as well as those of other agencies.

This report summarizes each of these areas of research in some detail, but the interested reader is referred to the series of semi-annual progress reports published during the term of this

grant for more detail. Those personnel at Georgia Tech who have worked on this grant are grateful to NASA for long-term support in a rapidly-changing and very challenging research discipline.

## 1. Introduction

### 1.1 Background

This document is the final report on NASA grant NSG-5012 "Research in Millimeter Wave Techniques", which is designated at the Georgia Institute of Technology as Project A-1642. This program was initiated in June, 1974 and continued through the fall of 1986, making it one of the longest running projects in the history of the Georgia Tech Research Institute (GTRI). When this program was initiated at Georgia Tech, the Engineering Experiment Station was the organization responsible for conducting it, but the name of this organization was changed to GTRI in the fall of 1986. The initial project director at GTRI was Mr. J. W. Dees. He was succeeded in 1976 by Dr. R. W. McMillan, who was in turn replaced by Mr. R. E. Forsythe. Upon Mr. Forsythe's resignation from Georgia Tech in 1986, Dr. McMillan was again appointed project director until the end of the program. The late Mr. J. Larry King was NASA Goddard technical monitor from the beginning of this program until his death in 1982. Mr. W. T. Walton served as program monitor during 1982/83, and Mr. L. R. Dod then directed this program until its termination in 1986.

### 1.2 Summary of Areas of Investigation

During the twelve years in which this project was active, almost every area of millimeter wave (MMW) research was touched upon in some way. At the beginning of the program, special emphasis was placed on the study of propagation and radiometry in the MMW bands because of NASA's great interest in remote sensing. Later emphasis was placed on the development of advanced MMW componentry, including devices developed both in waveguide and quasi-optical media. These developments have been of great benefit both to other programs at Georgia Tech and to programs at

other agencies conducted by other contractors. Several very useful applications of the technology developed with support from this grant are still being made at Georgia Tech and elsewhere.

In the areas of atmospheric research related to propagation and radiometry, calculations of atmospheric attenuation and radiometric antenna temperature have been made for frequencies throughout the MMW bands. These calculations have been supported by measurements of these parameters using propagation ranges and radiometers developed at Georgia Tech with support from this grant. Of special interest was the 183 GHz absorption in water vapor, which was studied during a series of flights by the NASA Convair 990 during the last few years. This transition was used to study water vapor profiles and map clouds, and a colocated 94 GHz instrument, together with instruments from other experimenters, was used for reference measurements. This actual series of airborne measurements was not supported by the grant, but technology developed with grant support was extensively used in the airborne measurements and in other NASA programs. This 183 GHz water vapor transition, which was extensively studied during the series of airborne measurements, was also studied using a ground-based radiometer. Radiometric and propagation calculations and measurements are discussed in more detail in Sections 2 and 3.

Perhaps the most interesting and useful contribution made by this project is in the development of high-performance MMW mixers, and the subharmonic mixer developed for the 183 GHz radiometers is an excellent example of this technology. This device was fabricated on quartz stripline, and used back-to-back point-contact Schottky-barrier diodes to generate only the even harmonics of the LO input for mixing with the fundamental signal frequency. This mixer has the advantage of using a subharmonic LO without the poor conversion loss usually associated with harmonic mixers. A variant of this device is designed to operate

from the fourth subharmonic of the LO, thus providing means for extending methods of fabrication of totally solid-state receivers far into the submillimeter range of the frequency spectrum. Mixers fabricated at Georgia Tech for the NASA programs were capable of a conversion loss of 5.5 dB at 183 GHz. An f/4 subharmonic mixer designed and built for an Army radar operating at 225 GHz had a conversion loss of 8.5 dB, and a 340 GHz version is being designed and built for another Army program. Section 4 of this report discusses the design and performance of these mixers.

Some very interesting results in the area of MMW quasi-optics have been obtained during this program. An area of particular interest was the fabrication of MMW optical diplexers for mixing signal and local oscillator (LO) beams into a mixer. In the process of studying these devices, some potentially useful properties of wire grid arrays were derived, and were later verified by measurements. These arrays were found to behave as tunable bandpass or band reject filters for the MMW frequency bands, and were also quite easy to fabricate. Section 5 discusses the derivation of the properties of these grids, and presents the results of measurements of bandpass filters fabricated from them.

Based on this brief introduction, it is easy to see that NSG-5012 has made significant contributions to many areas of MMW technology, and that these contributions have benefited other government agencies besides NASA as well as being of great benefit to Georgia Tech. The following sections of this report give examples of each of these areas of study and accomplishment.

## 2. Calculations of Atmospheric Attenuation and Radiometric Antenna Temperature

One of the earliest efforts associated with this NASA grant at Georgia Tech was the calculation and measurement of atmospheric attenuation coefficients and radiometric antenna temperatures. These studies were designed to support the NASA remote sensing programs with the ultimate goal of building a radiometer to operate on the 183 GHz water vapor absorption from space, and thus to provide worldwide information about atmospheric water vapor profiles. This type application provided the motivation for the development of the subharmonic mixers, discussed briefly in Section 1 and to be discussed in more detail in Section 4, since these devices provide a basis for the fabrication of all solid-state receivers. This section details the calculation of attenuation coefficients and antenna temperatures, and the next section compares the results of these calculations to experiment.

Van Vleck and Weisskopf [1] have shown that the attenuation coefficient  $\alpha_0$ , at frequency  $\nu$ , for a collision-broadened absorption line centered at frequency  $\nu_0$ , with linewidth parameter  $\Delta\nu$ , is given by

$$\alpha_0 = \frac{8\pi^2 N n |\mu|^2 \nu_0 [\exp(-E_i/kT) - \exp(-E_f/kT)]}{3hcG} F(\nu) \quad (1)$$

where the other parameters are determined as discussed below. The parameter  $N$  is the number of molecules per unit volume and is

$$N = \frac{N_A \rho}{M} \quad (2)$$

in which  $N_A$  is Avogardo's number,  $\rho$  is the density of molecules, and  $M$  is the number of grams in a gram molecular weight. For water, this number is  $N = 3.346 \times 10^{16}$ , where  $\rho$  is measured in

$\text{g/m}^3$ . The factor  $|\mu|^2$  is the square of the dipole matrix element between transition states and is equal to  $\sum |\phi|^2 \mu_0^2$  where  $\mu_0^2$  is the electric dipole moment. The factor  $\sum |\mu|^2$  is the line-strength parameter determined by King et al. [2], and  $\mu_0^2$  is  $3.39 \times 10^{-36}$  ESU from Van Vleck [3]. The statistical weighting factor  $n$  which accounts for nuclear spin is unity [4] for even rotation states and 3 for odd rotational states. In the exponential terms  $E_i$  is the energy of the lower transition state,  $E_f$  is the energy of the upper state,  $k$  is Boltzmann's constant, and  $T$  is the absolute temperature at which the attenuation is measured. The partition function  $G$  has been calculated by Van Vleck [3] to be 170 at 293K and varies with temperature as

$$G = KT^{3/2}. \quad (3)$$

Evaluation of the constant  $K$  from the previous values gives  $G = 0.0339T^{3/2}$ .

The line shape factor  $F(\mu)$  derived by Van Vleck and Weisskopf is given by

$$F_{\nu\nu-W}(\nu) = \left(\frac{\nu}{\nu_0}\right)^2 \left[ \frac{\Delta\nu}{(\nu - \nu_0)^2 + \Delta\nu^2} + \frac{\Delta\nu}{(\nu + \nu_0)^2 + \Delta\nu^2} \right] \quad (4)$$

where the parameters are defined as before. Another analytical line shape factor was derived by Gross [5], who took account of the fact that the duration of collision of the molecules is short compared to the resonant period of the line, which is the case for foreign-gas broadening. This factor is given by

$$F_G(\nu) = \frac{4\nu^2 \Delta\nu}{(\nu_0^2 - \nu^2)^2 + 4\nu^2 \Delta\nu^2}. \quad (5)$$

Although there is little difference in the millimeter-wave spectral region between results obtained using (4) and (5), the latter result will be used for some of the calculations discussed in this report, because of its more general nature.

Unfortunately, neither of the above analytical line shapes gives good agreement with experiment in the atmospheric transmission windows, giving generally lower attenuation values than are observed. In order to fit calculations to experimental data, at least two empirical corrections to the above line shapes have been proposed. Schulze and Tolbert [6] have used the expression

$$F_{S-T}(\nu) = \left( \frac{\nu}{\nu_0} \right)^2 \frac{\Delta\nu^{0.65}}{|\nu - \nu_0|^{1.65} + \Delta\nu^{1.65}} \quad (6)$$

to fit calculated and observed absorption values for the 118.6 GHz oxygen line. This expression has the same value at the center of the line as the Van Vleck-Weisskopf and Gross line shapes, but gives greater absorption in skirts of the lines. It was formulated to account for the finite collision time between molecules, but is again not very satisfying because it is empirical. A modification to the Gross line shape, based on the assumption of a continuum absorption, has been proposed by Gaut and Reifenstein [7], who use the expression

$$\Delta\alpha = 1.08 \times 10^{-11} \rho \left( \frac{300}{T} \right)^{2.1} \left( \frac{P}{750.2} \right) \nu^2 \text{cm}^{-1} \quad (7)$$

where P is the atmospheric pressure in millimeters of mercury and  $\nu$  is in gigahertz. Note that this expression adds a continuum term proportional to the square of the frequency.

As an example of this type of calculation, the zenith attenuation at 230 GHz was calculated for comparison to experimental observations made by G. T. Wrixon at Bell Laboratories in Holmdel, N. J., who served as a consultant to this program [8]. The results of these calculations will be given in the next section, but the water vapor and temperature distributions used will be discussed in this section as part of the theory of these calculations.

Since a calculation of zenith absorption must include the effects of altitude, the altitude dependence of terms in (1) must

be considered. The water vapor density is assumed to vary as shown in Fig. 2-1, in which the plotted points are averages of water vapor density distributions for the months of October and November 1973, measured by radiosonde at the John F. Kennedy Airport in New York, NY, which is 80 km from the measurement site. The solid lines indicate extremes of water vapor distributions used in these calculations which were varied according to on-site measurements of ground-level water vapor density. Since the radiosonde measurements were made only to a level of 10 km, the solid-line distributions were extrapolated to 50 km consistent with the 50-km upper limit of the calculations. This extrapolation ignores any possible contribution to attenuation caused by stratospheric water vapor, which has been treated by Croom [9], [10], and by Barrett and Chung [11]. This high altitude water vapor is expected to make a negligible contribution to attenuation in the 230 GHz window, however, because the low pressure makes the lines very narrow.

The temperature profile used in these calculations is also based on an average of the radiosonde data for the months of October and November, and is shown plotted in Fig. 2-2. Again, the indicated extrapolation to 50 km is made, and is considered valid because temperature at the higher altitudes is expected to have little effect on total zenith attenuation. The low-altitude slope of the temperature distribution curve was varied according to on-site measurements of ground-level temperature; otherwise, the same distribution was made for all calculations. Water vapor and temperature profiles used for other calculations in Section 3 are similar to those of Figures 2-1 and 2-2.

From Barrett and Chung [11], the pressure dependence at altitude  $Z$  is taken to be

$$P = 760(10^{-3.05Z/50}) \quad (8)$$

and the linewidth parameter is

$$\Delta\nu = \frac{\Delta\nu_0(P/760)(1+0.0046\rho)}{(T/318)^{0.625}} \quad (9)$$

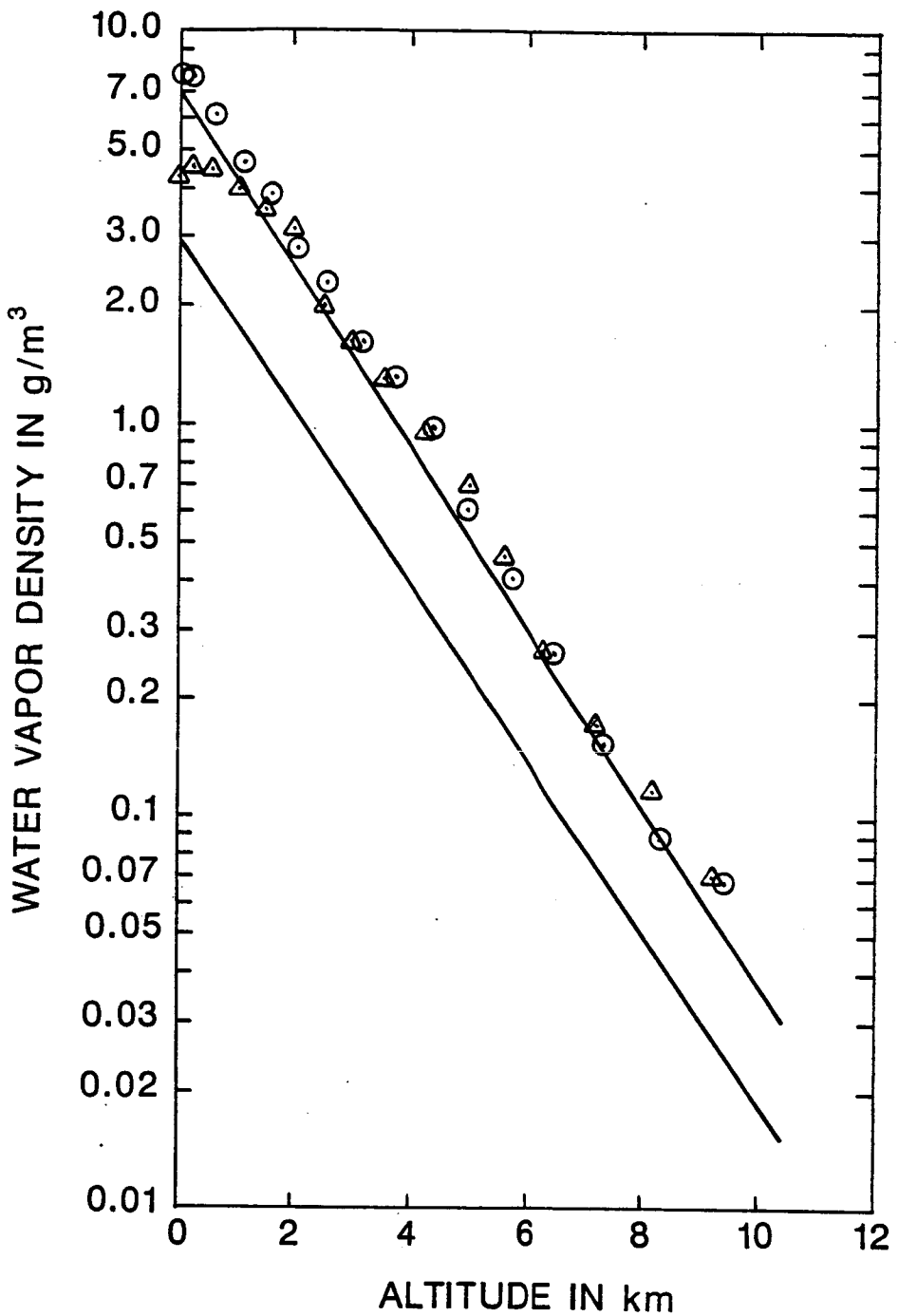


Figure 2-1. Water vapor density vs. altitude measured by radiosonde at Kennedy Airport, and used for zenith attenuation calculations at 230 GHz.

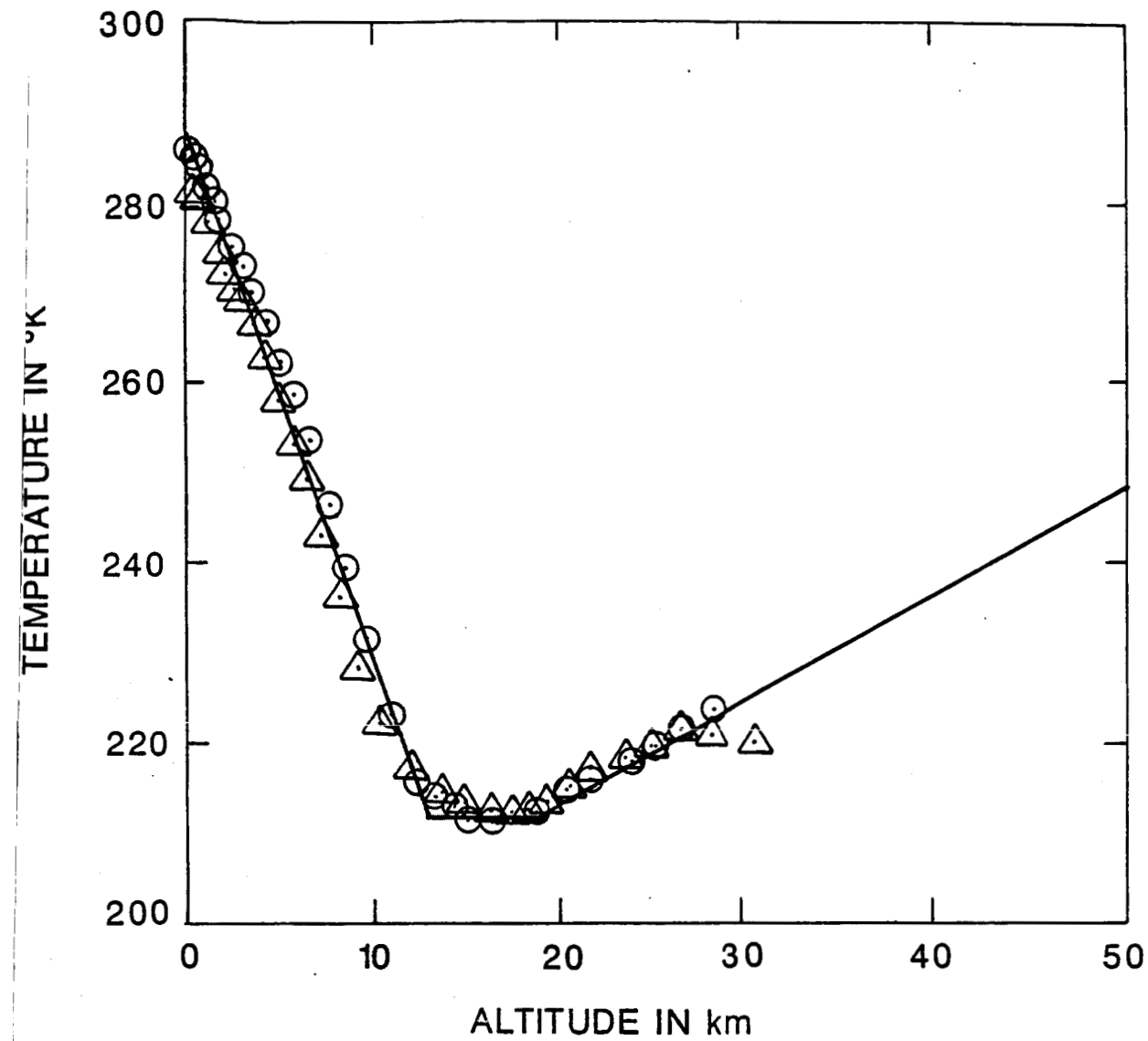


Figure 2-2. Atmospheric temperature profile at Kennedy Airport used for zenith attenuation calculation at 230 GHz.

where  $\Delta\nu_0$  is the linewidth parameter at P=760 mm and T=318K for small  $\rho$ .

The total atmospheric attenuation measured looking upward from altitude  $h$  at zenith angle  $\theta$  is given by

$$\gamma = \exp\left(-\int_h^\infty \alpha'(Z) \sec \theta dZ\right). \quad (10)$$

Three cases are now considered: (1)  $\alpha'=\alpha_0$  and the Schulze-Tolbert line shape (6) is used for  $F(v)$  to calculate  $\gamma$ , (2)  $\alpha'=\alpha_0+\Delta\alpha$  and the Gross line shape (5), together with the continuum expression (7) for  $\Delta\nu$  is used to calculate  $\gamma$ , and (3)  $\alpha$  is calculated using the unmodified Gross line shape. In making these calculations, contributions due to the 24 strongest water vapor absorption lines up to a frequency of 916 GHz were considered. The attenuation due to the 118.6 GHz oxygen line was also added. The calculations covered a frequency range of 190-270 GHz, which includes the maximum transmission band of the 230 GHz window. Equation (10) was numerically integrated using the values of  $\alpha$  from the three cases discussed above with the maximum altitude taken to be 50 km. In order to get good accuracy and minimize computer time, the widths of the atmospheric strata  $\Delta Z$  were varied from a minimum of 2.5 m at low altitude to a maximum of 50 m at high altitude, in performing the integration. These calculations will be compared to experiment in the next section.

It is a general characteristic of calculations of this type that they do not agree well with measurements of attenuation. The reason for this disagreement is usually ascribed to our inability to account for the contributions of the skirts of the literally thousands of water vapor transitions which have center frequencies extending all the way to the near infrared portion of

the electromagnetic spectrum, with many of them having individual attenuation coefficients on the order of thousands of dB per kilometer, making the water vapor absorptions perhaps the most dominant features in atmospheric absorption. Many attempts have been made to account for this lack of agreement empirically, with the correction by Gaut and Reifenstein mentioned above being perhaps the most well known. More recently, the careful experimental and analytical work of Liebe [12] has resulted in an empirical correction that has given excellent agreement with experimental measurements of attenuation for a wide variety of atmospheric conditions for the range of MMW frequencies extending up to above the 230 GHz atmospheric window. Although empirical corrections are not usually very satisfying, it does not appear likely that an accurate theoretical solution will ever be possible because of the extremely large numbers of minute corrections to absorption by thousands of water vapor transitions that must be accurately considered by any theory. The usefulness of the empirical solution is further supported by the fact that it gives good results.

During the last few years, there has been some evidence for so-called anomalous absorption in the MMW frequency region. This absorption has been observed by Gebbie and coworkers [13], and is apparently associated in some way with conditions of high humidity, and possibly the onset of fog. Initial attempts to explain this type absorption considered water vapor dimers as its cause, but studies of these dimers showed that the energy levels did not agree with those required to explain the observed phenomena. Carlon [14] has attempted to explain this phenomenon by considering the formation of clusters of water vapor molecules, which might be considered as incipient fog droplets, but no satisfactory explanation has been advanced to date by anyone. Most recently, questions have arisen as to whether or not anomalous absorption has ever been observed at all,

especially in view of the success of Liebe [12] in explaining measured atmospheric absorption in the MMW frequency bands.

To summarize this section, it appears that the state of the theory of transmission through the atmosphere at MMW frequencies is very good, but the agreement between theory and experiment degrades as one considers higher frequencies, namely those above the 230 GHz window. With the possible exception of the 340 GHz window, these higher frequencies are of little interest for atmospheric remote sensing in any case, although higher frequency windows might be usable by high altitude sensors such as those mounted on mountain tops, aircraft, or balloons. At high altitudes, the water vapor density is much lower with resulting lower absorption, and the contributions of the skirts of the higher-lying absorption lines are also smaller, so that atmospheric absorption is much less of a problem.

### 3. Results of Calculations and Measurements of MMW Attenuation Coefficients and Radiometric Antenna Temperatures

#### 3.1 Calculations

Using the formalism described in the last section, it is possible to calculate the attenuation coefficient for propagation of MMW radiation through the atmosphere, subject to the limitations discussed in the last section. Based on the horizontal attenuation coefficient, which is known as a function of altitude, it is possible to calculate the total attenuation through the atmosphere and the radiometric antenna temperature of the atmosphere as functions of zenith angle. It is of special interest to make these calculations as a function of frequency, because the results clearly show the atmospheric windows, which appear as regions of low attenuation or low antenna temperature. The attenuation varies linearly with atmospheric water vapor density, a parameter that is taken to be  $7.5 \text{ g/m}^3$  for a standard atmosphere, but which may vary from 1 or  $2 \text{ g/m}^3$  in the Arctic to more than  $20 \text{ g/m}^3$  in the tropics. The results presented in this report were all calculated for  $7.5 \text{ g/m}^3$ , unless otherwise noted.

Figure 3-1 [15] shows the result of calculating the horizontal atmospheric attenuation over the range 150-700 GHz. It must be noted that a slight error was made in making these calculations, and the values of attenuation tend to be lower than observed for this reason. The consequences of this error are especially evident in the window regions of the spectrum, where the attenuation calculated is somewhat lower than that measured, but the attenuations calculated on the line peaks agree well with measurement. This lack of agreement in windows and good agreement on peaks results from the reduced contributions of the skirts of the higher-lying lines as a percentage of the total attenuation on the peaks, while these contributions have a higher

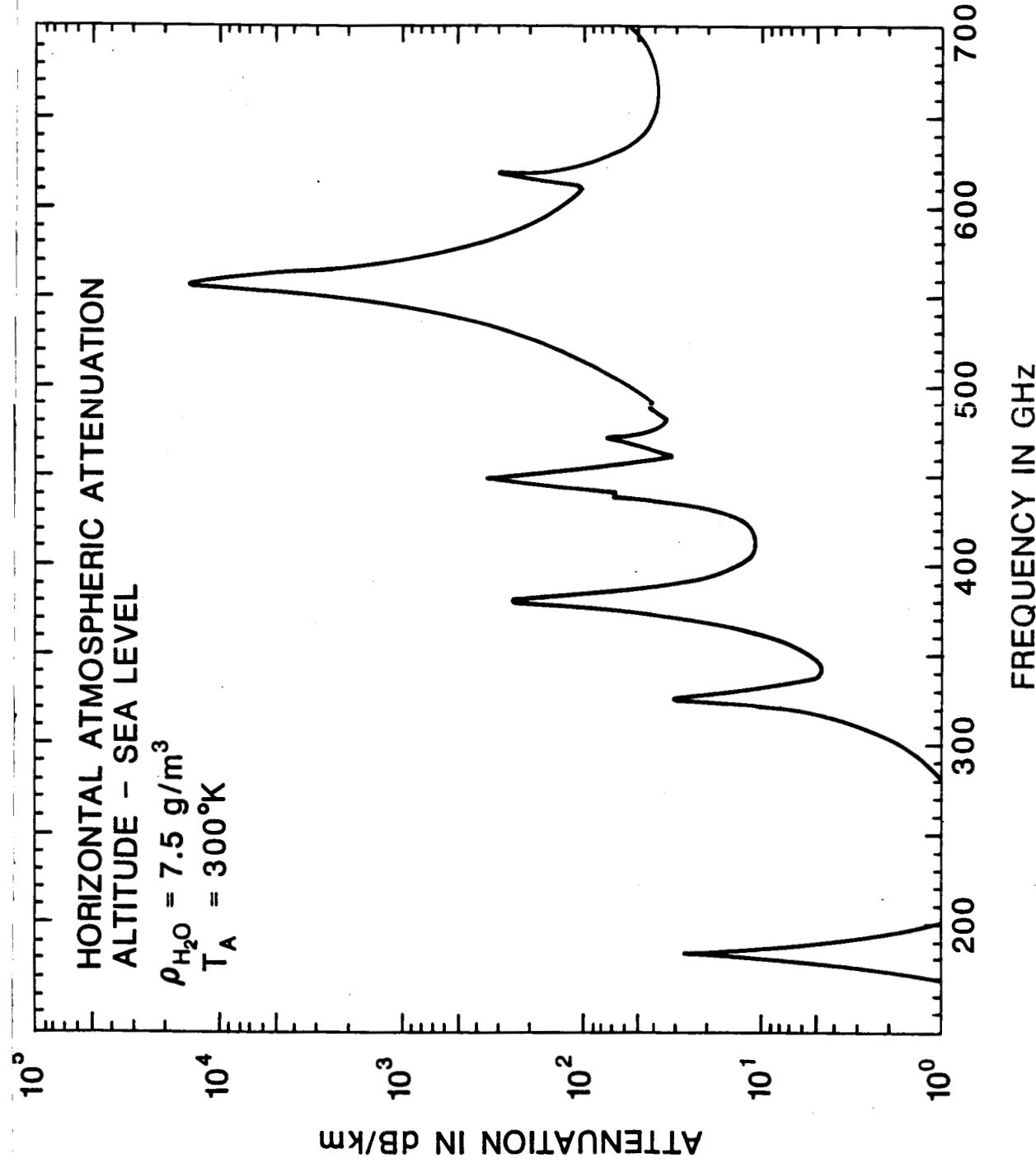


Figure 3-1. Calculated horizontal atmospheric attenuation due to water vapor as a function of frequency.

percentage contribution in the windows. This phenomenon is observed in every calculation that does not make use of an empirical correction for the contributions of the higher-lying lines, but is more evident in the case presented in Figure 3-1 because of the added effects of the slight error in calculation. In Figure 3-1 and in every figure in this section, the qualitative features of the spectra, which give the locations of the absorption peaks and the windows, are accurate. Note the extremely high absorption (greater than  $10^4$  dB/km) on the transition at 556 GHz. There are many more stronger absorptions at higher frequencies, and the combined magnitude of these attenuations render much of the far-infrared bands useless for propagation at sea level, although the window regions would be useful at very high altitude. On the line peaks, the attenuation is so large that these peak frequencies would only propagate in space.

Figure 3-2 [15] shows the total atmospheric attenuation from sea level at zero zenith angle. This graph has the same shape as the horizontal attenuation in Figure 3-1, but the attenuations are predictably higher. Again, the attenuations plotted for the window regions tend to be lower than observed. Figure 3-3 [15] shows the calculated zenith antenna temperature as a function of frequency, showing that the sky is cold in the window regions and approaches the sea-level ambient temperature on the absorption peaks. This result would be obtained for clear weather. In turbid weather, the sky temperature would tend to be uniformly warm, and might even approach a uniform temperature near the ambient temperature for the case of a heavy fog. These results have been verified experimentally at selected frequencies in the window regions by numerous radiometric observations at Georgia Tech, many of them supported by this grant or one of its offshoots.

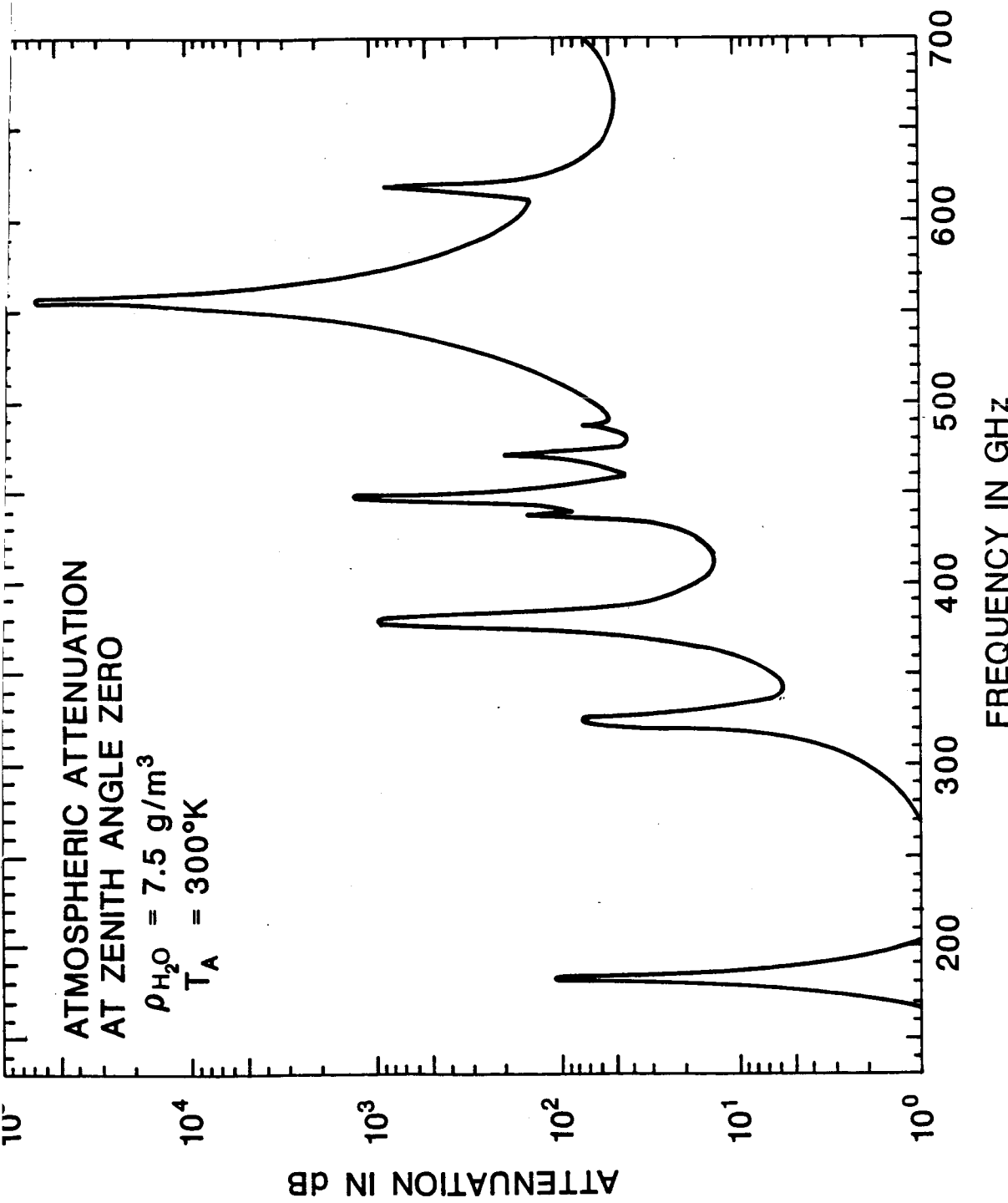


Figure 3-2. Calculated total zenith attenuation from sea level for the range 150-700 GHz under the same conditions as used for Figure 3-1.

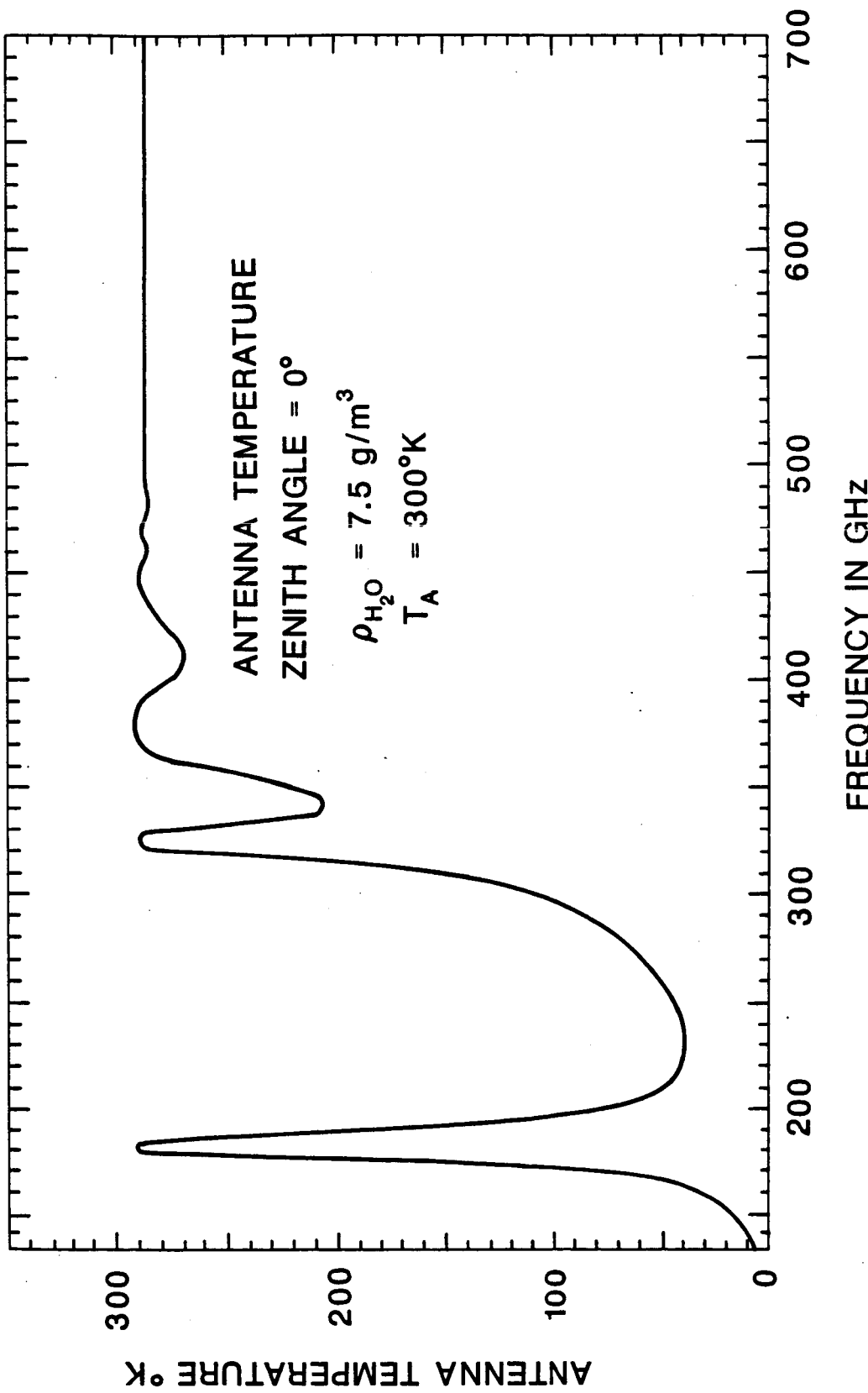


Figure 3-3. Calculated zenith antenna temperature in the range 150–700 GHz under the same conditions as used for Figure 3-1.

A useful method of measuring total atmospheric attenuation is to view the sun through the atmosphere with a radiometer, thus effectively using the sun as a transmitter source for these observations. Figure 3-4 [15] shows the results of calculating the antenna temperature expected when operating in this mode. In the window regions, where attenuation is lowest, the radiometer sees the temperature of the sun's surface attenuated only slightly by the water vapor in the atmosphere, but at the higher frequencies, the sun's radiation is almost completely attenuated, and one observes the temperature of the atmosphere reduced slightly by the fact that the radiometer sees a short distance into the atmosphere where the air is slightly cooler.

In using the formalism developed above to consider what happens when the atmosphere is viewed from above by a scanning radiometer, one obtains a very interesting result, as shown in Figure 3-5 [16]. Sharp peaks corresponding to the absorption lines are observed, followed by a minimum in temperature as the frequency is varied from the line peak, followed by a return to a higher temperature as the frequency is further varied. Although puzzling at first glance, this behavior has a simple explanation if one considers the temperature and water vapor profiles shown in Figures 2-1 and 2-2 and used for these calculations. On the peak of the line, the radiometer sees only a very short distance into the atmosphere, because of a high concentration of water vapor as shown in Figure 2-1. But the temperature at high altitudes is high according to Figure 2-2, so that the radiometer sees a high temperature. At frequencies slightly off line center, the radiometer sees further into the atmosphere because the attenuation is smaller, but by Figure 2-2 the temperature is lower at these lower levels, and the radiometer sees a minimum temperature. Finally, at frequencies further removed from the peak, the radiometer sees even further into the atmosphere, where

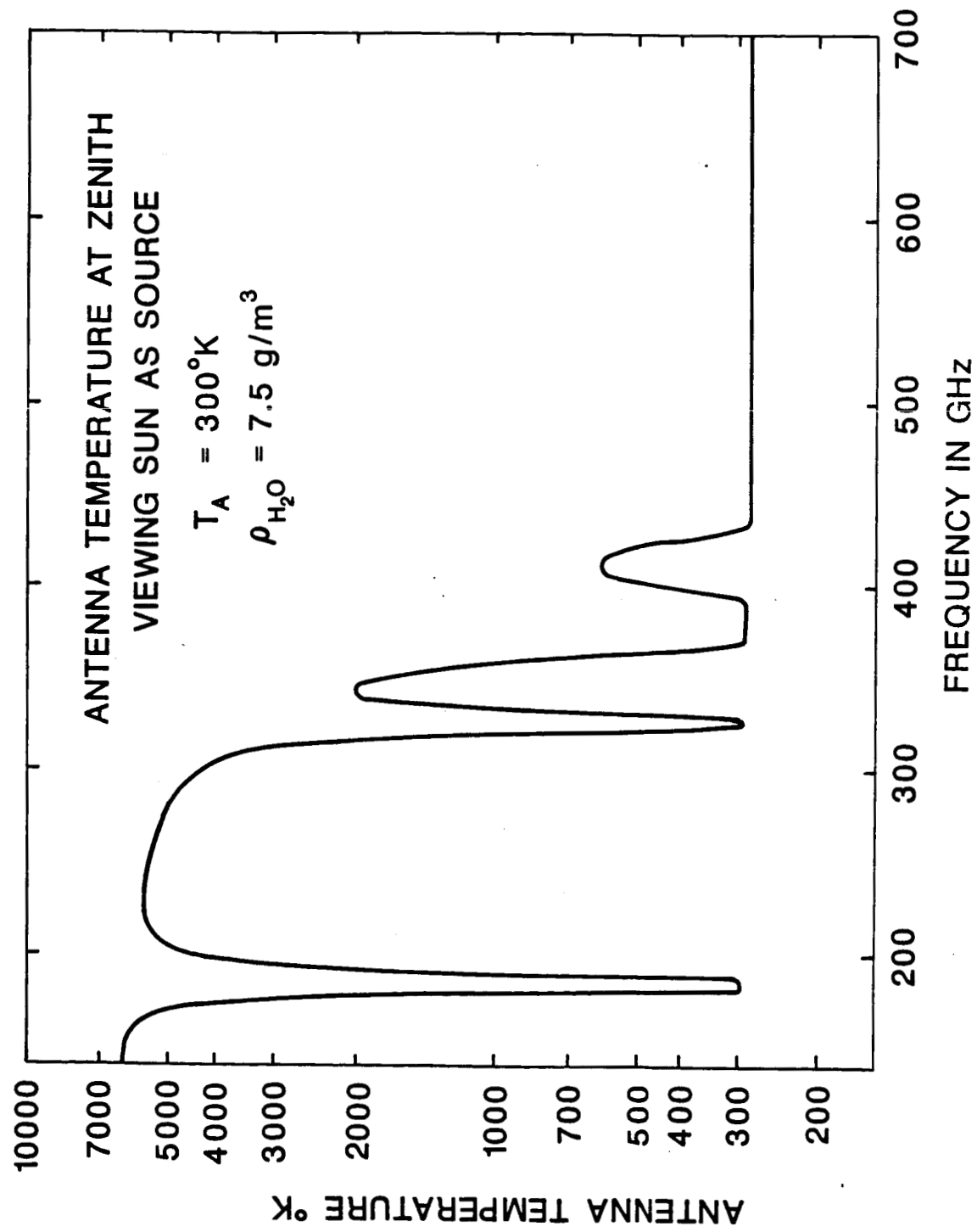


Figure 3-4. Calculated clear-air zenith antenna temperature viewing the sun as a source.

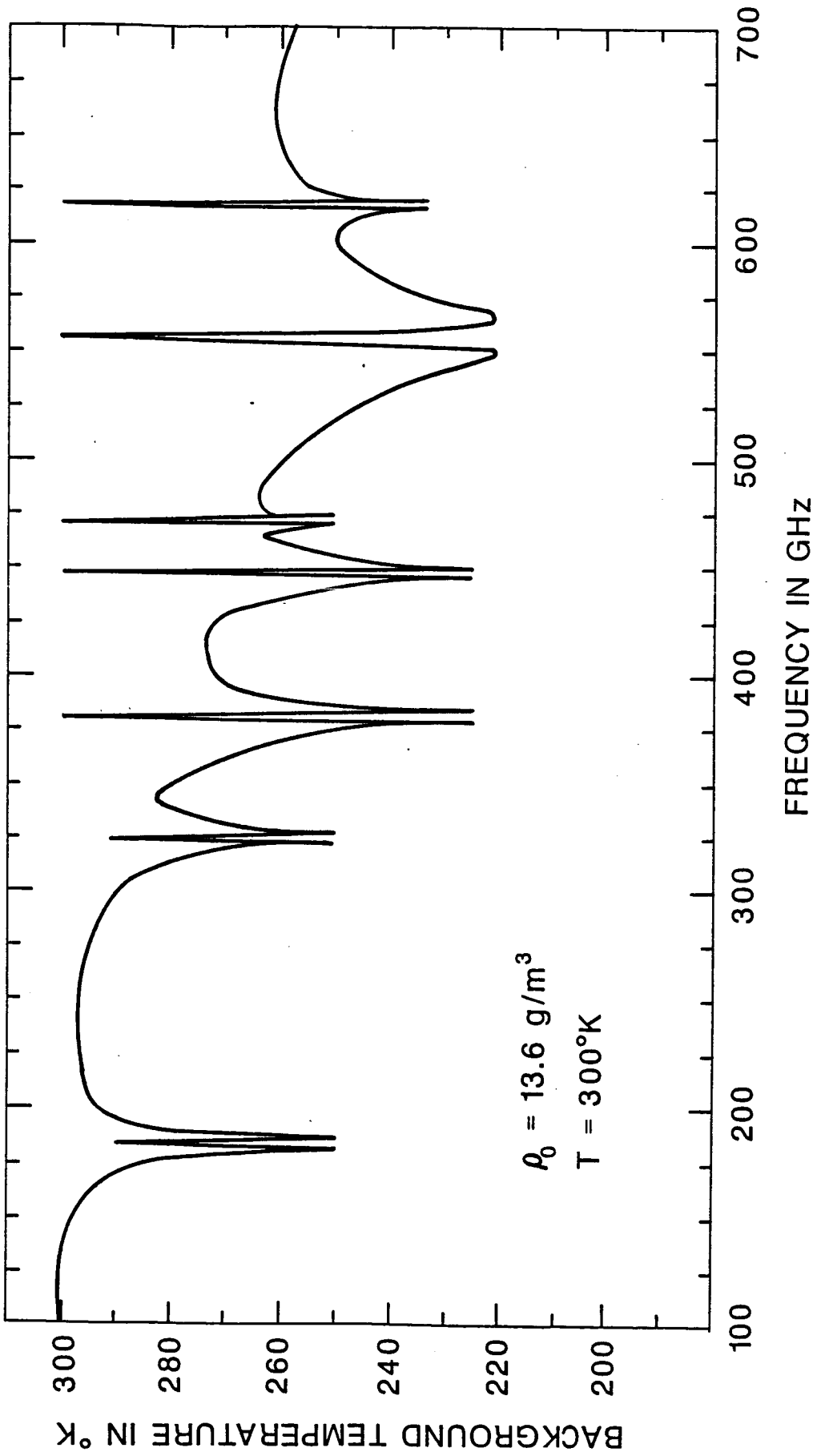


Figure 3-5. Calculated antenna temperature looking down from 50 km. The conditions are indicated on the figure.

the temperatures are again higher, resulting in higher measured temperatures at frequencies further removed from the peak. This behavior was apparently first predicted by Croom [10], and independently by Gallagher and McMillan [16], and has not been observed experimentally to the author's knowledge.

If the peak in radiometric antenna temperature discussed above is to be observed, stratospheric water vapor must be present. Otherwise, the radiometer sees down to colder levels on the line peak, and at frequencies removed from the line peak, it sees the warmer temperatures at lower levels. Figure 3-6 shows the result of calculating the antenna temperature for several different water vapor profiles as shown in Figure 3-7. Note that the peak in temperature occurs only when stratospheric water vapor is present; otherwise, the peak actually becomes a dip, as discussed above.

### 3.2 Measurements

#### 3.2.1 Attenuation Measurements

For measurements of horizontal attenuation at MMW frequencies, a propagation link operating at 94 GHz was set up between two buildings on the Georgia Tech campus. Figure 3-8 is a block diagram of this link and Figure 3-9 is a photograph of the transmitter end of this path. Transmitter and receiver were housed in a box with teflon windows as shown for all-weather operation. The transmitter was a reflex klystron oscillator and the receiver was a direct-detection type with a point-contact diode detector. Unfortunately, it was not possible to obtain meaningful attenuation data with this system because of the great difficulty in calibrating the measurement system. It is not difficult to make relative measurements of attenuation, but to make absolute measurements, one must exactly know the power

Water Vapor Density  $\rho_0 = 7.5 \text{ g/m}^3$

Ambient Temperature  $T_A = 300^\circ\text{K}$

Earth Reflectivity  $R = 0.1$

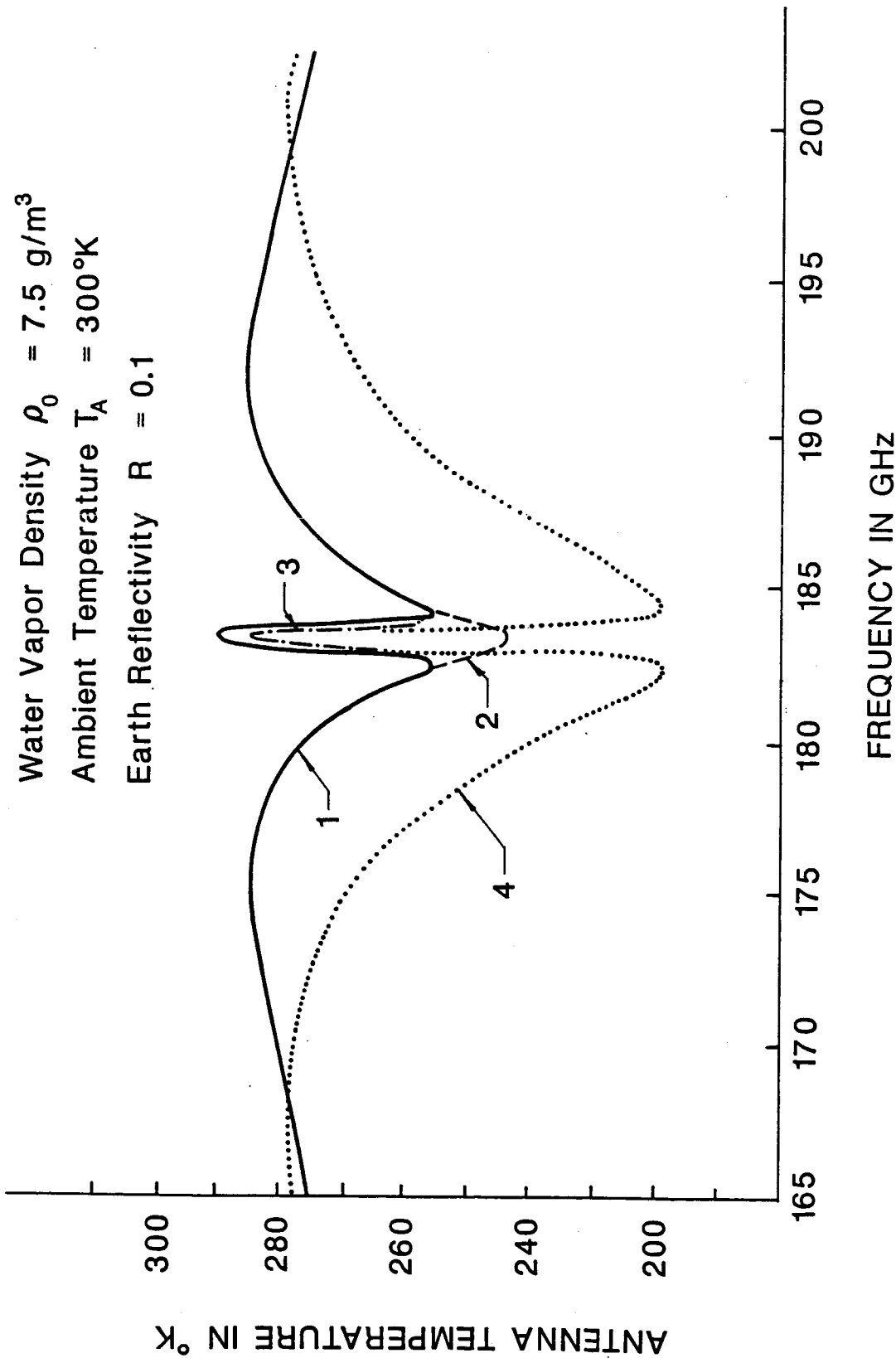


Figure 3-6. Calculated antenna temperature due to the 183 GHz water vapor transition viewed looking downward from 50 km. The numbers correspond to the different profiles of Figure 3-7.

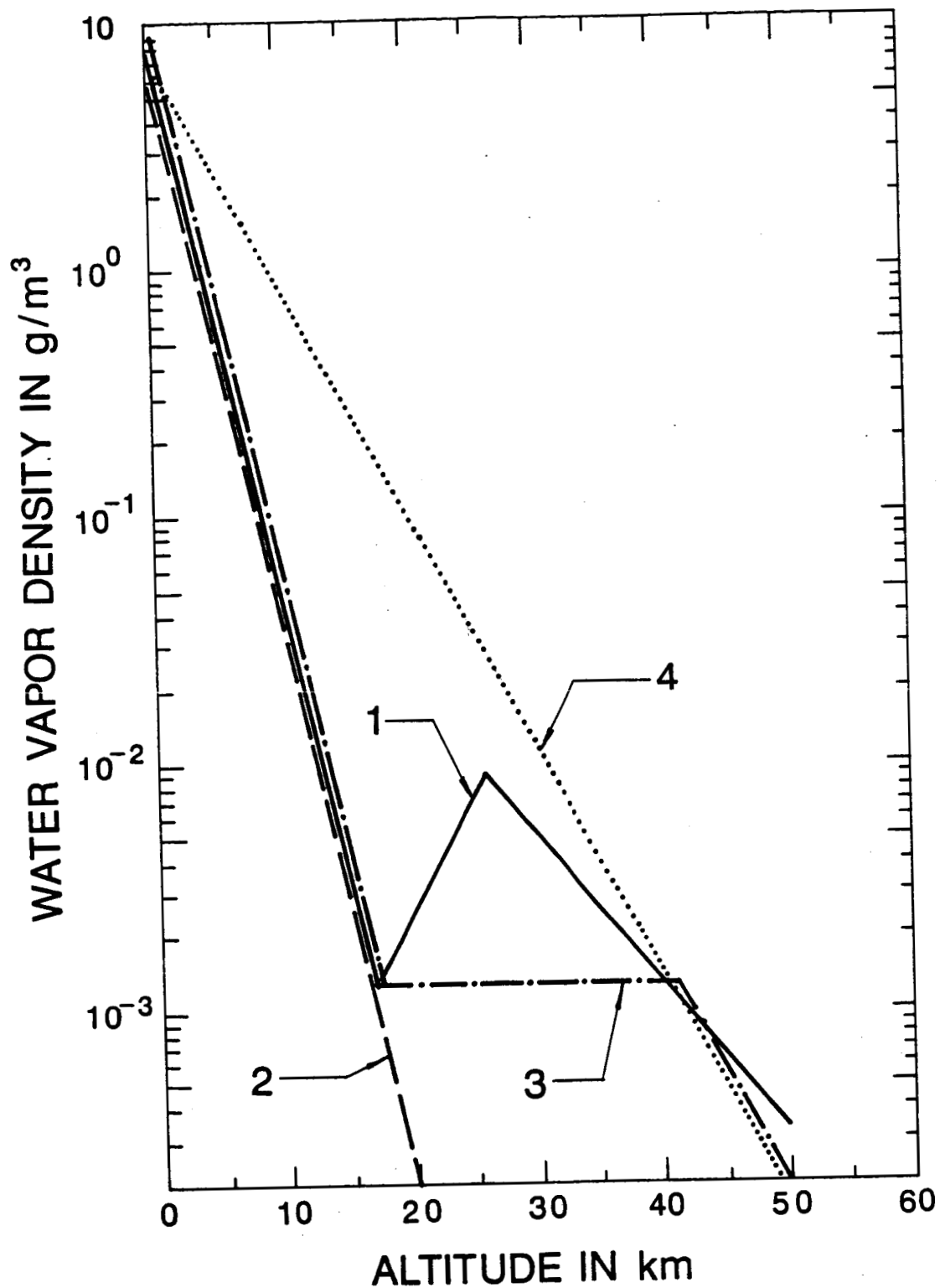


Figure 3-7. Atmospheric water vapor distributions used for the calculations shown in Figure 3-6. The numbers of the distributions correspond to the numbers on the curves of Figure 3-6.

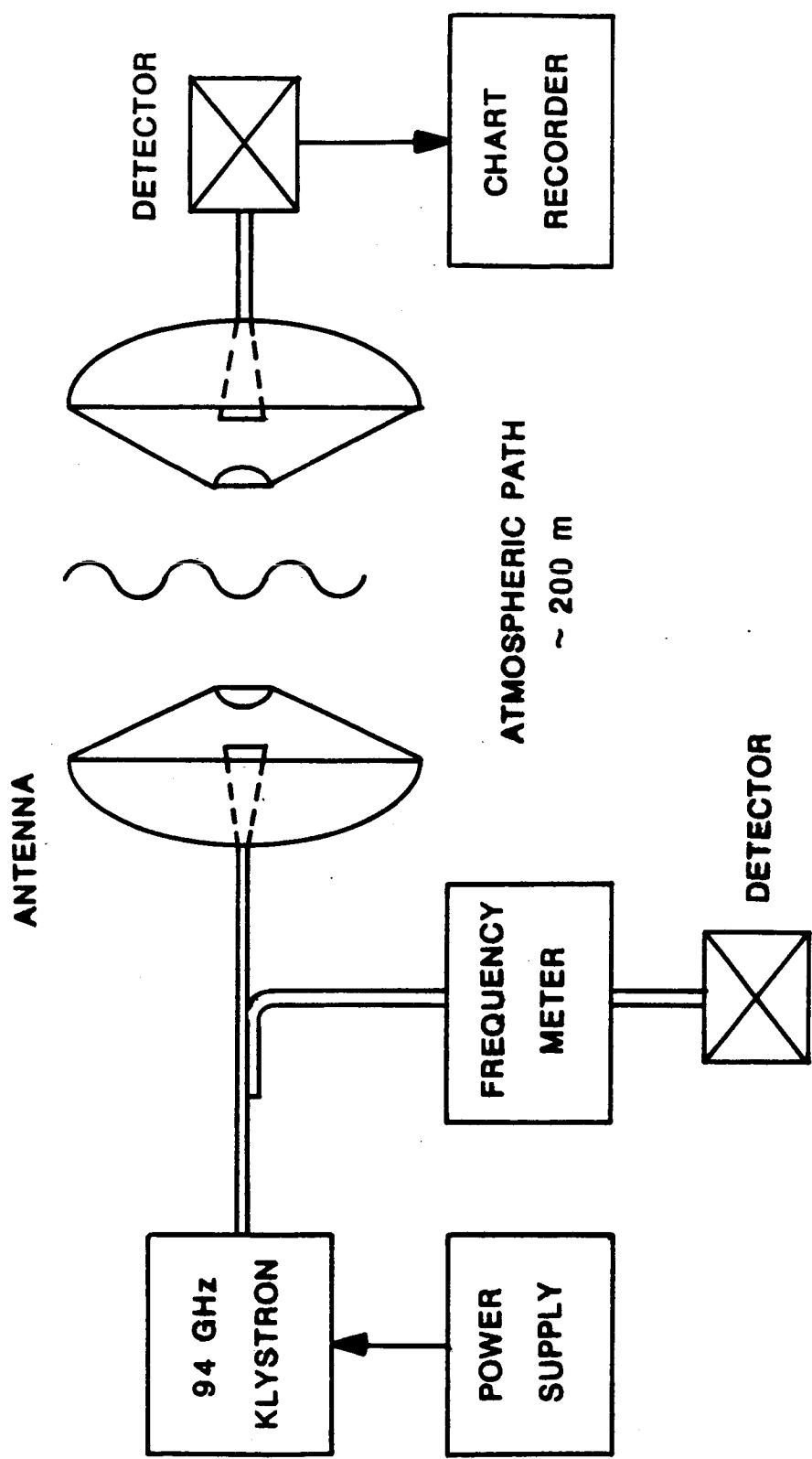


Figure 3-8. Diagram of MMW propagation link.

ORIGINAL PAGE IS  
OF POOR QUALITY

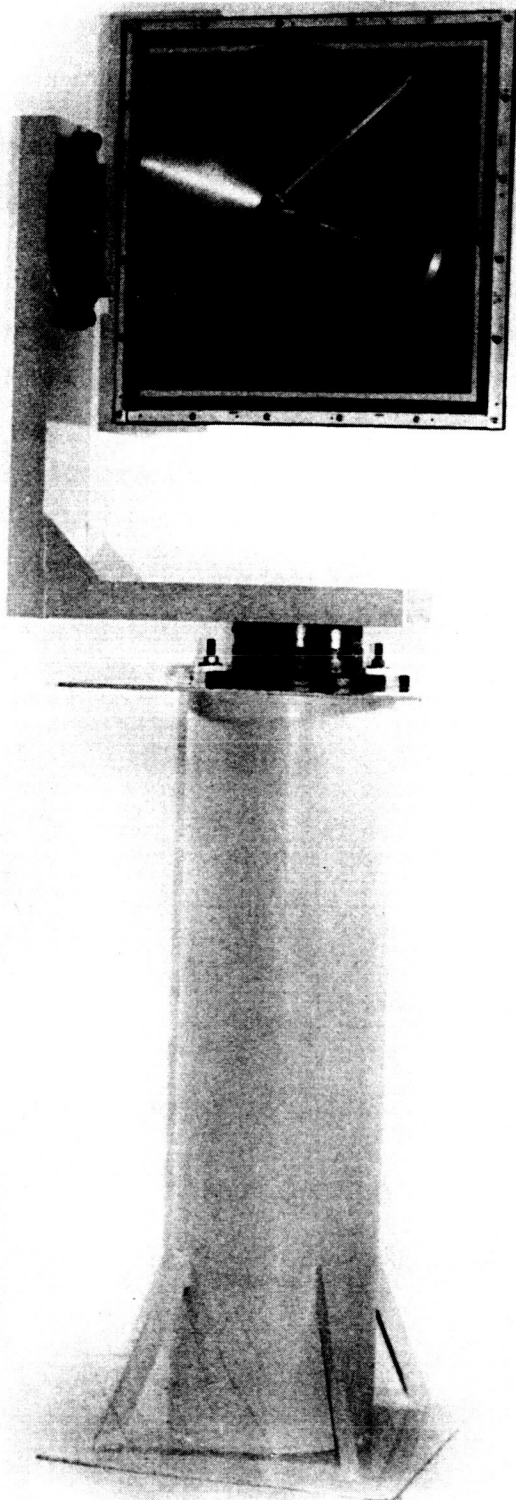


Figure 3-9. Photograph of transmitter end of propagation link. The antenna was housed in a teflon box for all-weather operation.

radiated by the transmitter, its antenna pattern, the fraction of incident power collected by the receiver, the receiver antenna pattern, and the detector sensitivity. Because of this array of potential problems, absolute attenuation measurements are made over two-way paths by using two or more calibrated reflectors (corner cubes) at different path positions to compensate for these effects. Because of these difficulties, meaningful measurements of absolute attenuation at MMW frequencies were not made.

### 3.2.2 Radiometric Measurements

A series of radiometric measurements of the 183 GHz water vapor transition were made early in this program, using the apparatus shown in Figure 3-10. At the time that these measurements were made, this radiometer was considered state of the art, but much more sophisticated devices are available at this time, and many of these new techniques are incorporated into radiometers built by Georgia Tech for NASA since that time. The system of Figure 3-10 used a cross-guide harmonic mixer fabricated by Custom Microwave of Longmont, Colorado, which was pumped by a 91 GHz reflex klystron oscillator. This radiometer was of the Dicke type, which means that the input radiation is mechanically chopped before being fed into the mixer. On alternate halves of the chopping cycle, the receiver views the scene of interest and the reference load. This radiometer is calibrated by placing an absorber of known temperature in front of the antenna and noting the displacement in output by the receiver.

The radiometer antenna is a corrugated horn which was fabricated by Custom Microwave by an electroforming process. The design and improvement of such horns has been a significant part of the contributions of this grant to MMW technology. The output

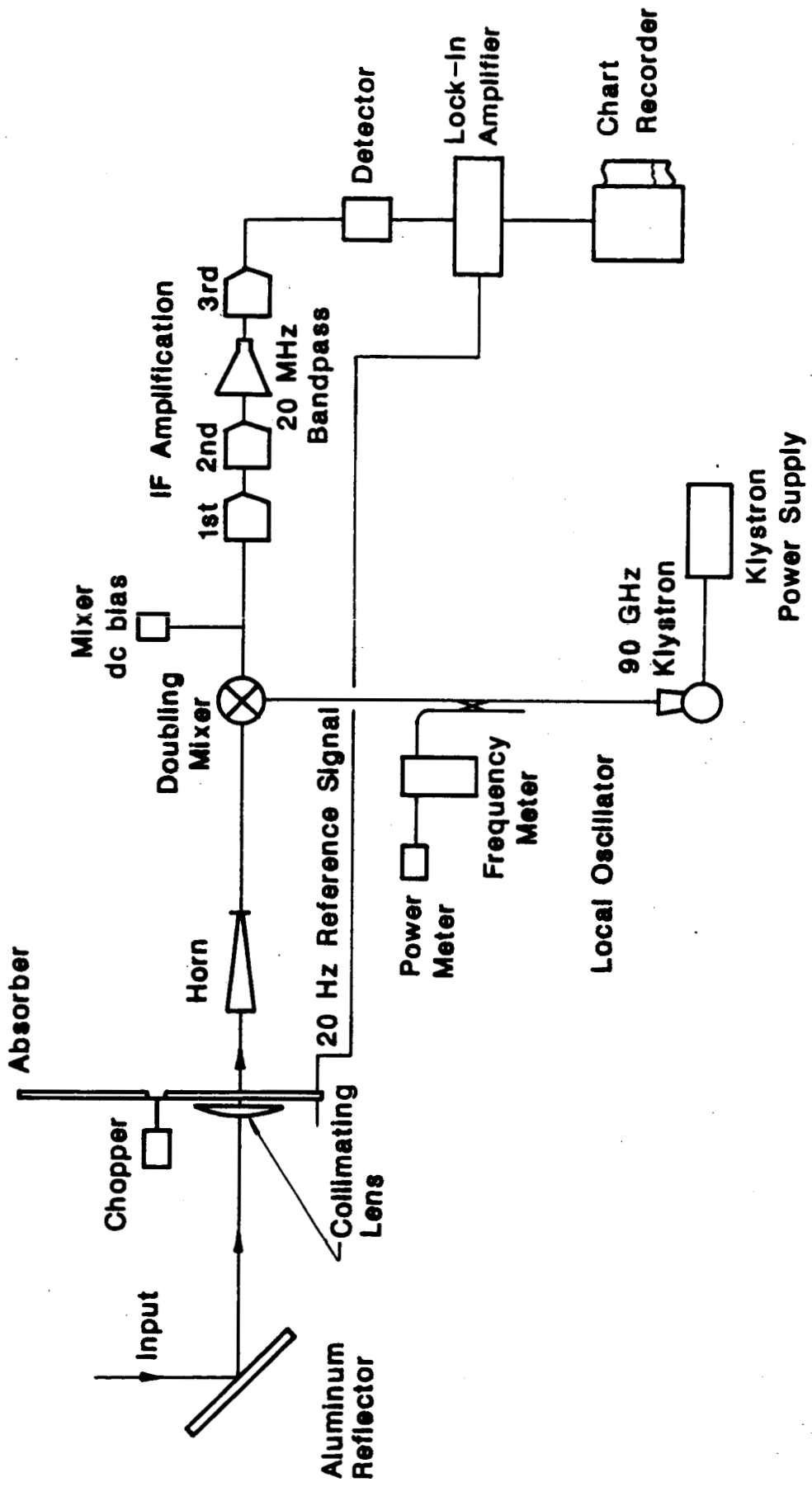


Figure 3-10. Block diagram of 183 GHz radiometer.

of the mixer is the intermediate frequency (IF) which is amplified in the IF amplifier and detected by a square law detector. The output of this detector is fed into a lock-in amplifier, where it is compared to the reference signal derived from the chopper and further amplified to drive the chart recorder. The radiometric antenna temperature is derived by scaling the chart recorder deflection and comparing it to that obtained by measuring the calibration load. Figure 3-11 shows the result of measuring the zenith antenna temperature at several frequencies near 183 GHz under the conditions specified in the figure caption. The circles are measured data, and the solid line was obtained by calculating the temperature using the techniques discussed in the last section. Notice that the water vapor line is broadened greatly by the combination of high temperature and extremely high absolute humidity. The agreement is considered to be plausible, except for the low-frequency portion of the spectrum. It must be remembered that the radiometer used for these measurements was probably the first built at the relatively high frequency of 183 GHz.

A series of measurements of total attenuation through the atmospheric was made at 230 GHz by G. T. Wrixon of University College in Cork, Ireland, while he was employed at Bell Laboratories. Dr. Wrixon served as a consultant to this grant for some time, and although these measurements were not supported by the grant, the calculations discussed in this section and comparison of these results to theory were grant-supported. These measurements used the sun as a source, and were made at a site in New Jersey a distance of 80 km from Kennedy Airport in New York City. Radiosonde data for ground truth were obtained from Kennedy. This experiment is described in detail in Reference [8], and Figure 3-12, taken from [8] shows typical results obtained and compares them to calculations of zenith

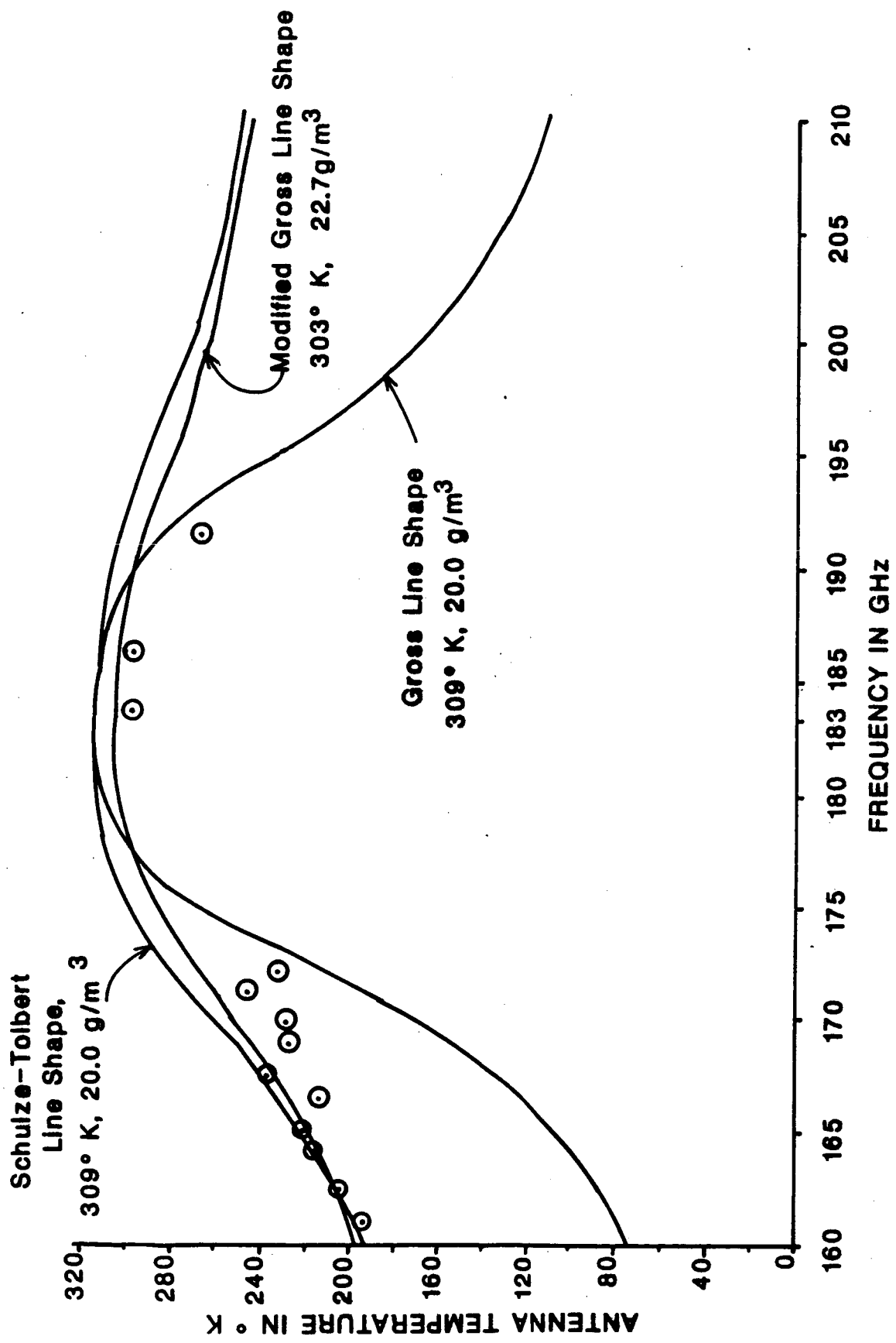


Figure 3-11. Results of measuring the antenna temperature near the GHz water vapor transition on a hot, humid summer day. Calculated values using various models are shown for comparison.

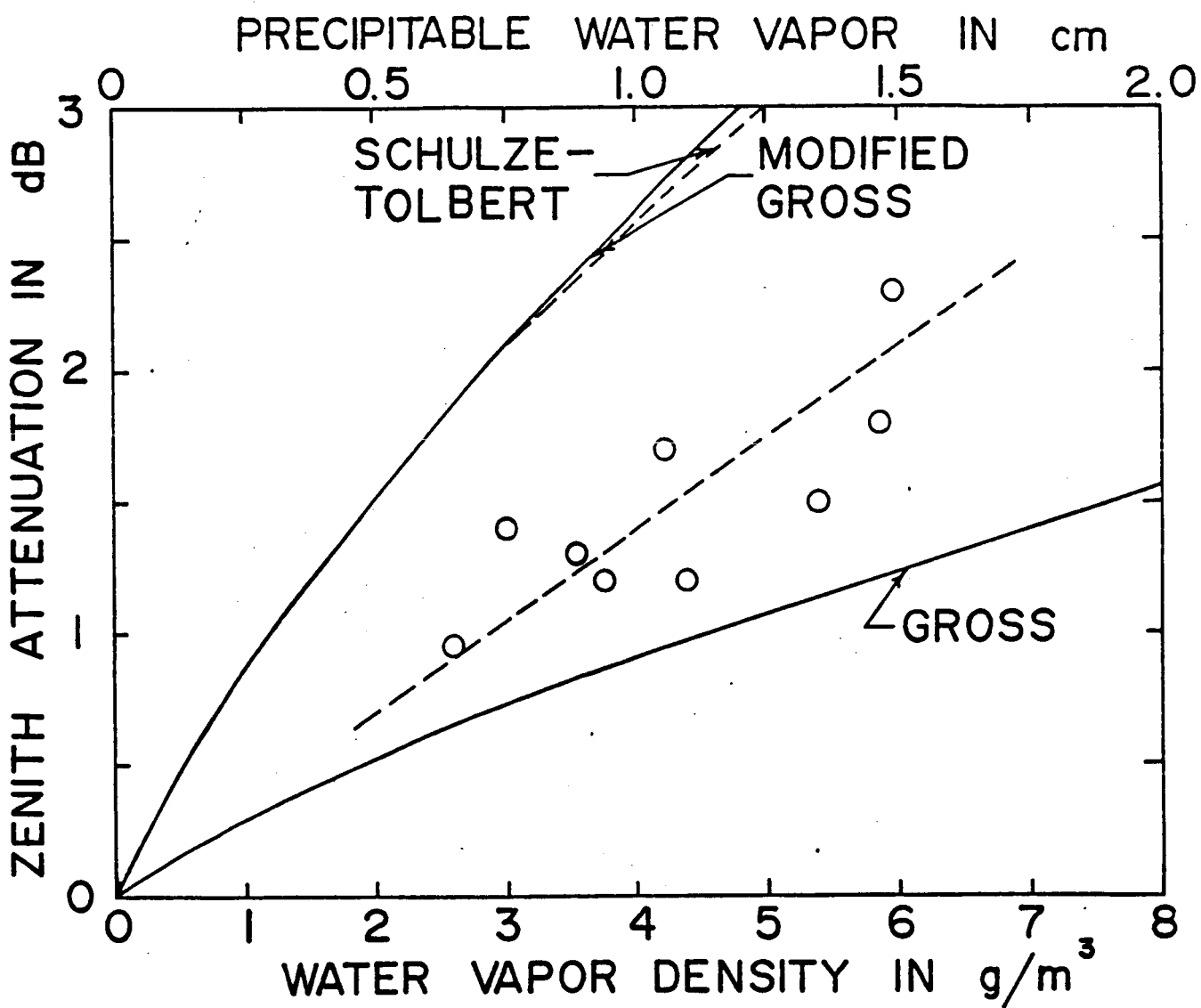


Figure 3-12. Comparison of calculated Zenith attenuation using various lineshapes to measured results. The dashed line represents the empirical relation  $A(\text{dB}) = 0.35\rho (\text{g}/\text{m}^3)$ .

attenuation made using the procedure described in the last section. Three sets of calculations are shown: (1) calculations were made using the Gross [5] analytical line profile, (2) these calculations were repeated using an empirical correction to the Gross profile suggested by Gaut and Reifenstein [7], and (3) a third calculation was made using an empirical correction to the original Van Vleck-Weisskopf [1] line profile devised by Schulze and Torbert [6] for the 118 GHz oxygen transition. The total zenith attenuation at 230 GHz is calculated as a function of water vapor density or total precipitable water vapor for the three cases cited above. These results show that none of the line shape theories used in this calculation, and considered to be valid at the time these calculations were made, give good results for the determination of atmospheric transmission. Since these calculations were made, Liebe [12] has made very careful and detailed calculations and measurements which have resulted in an empirical supplement to the analytical line shape model which gives excellent agreement with experiment over the whole range of MMW frequencies for almost all atmospheric conditions of interest.

It was indicated in an earlier section that absorbers or loads are used in radiometry for both calibration and reference. During early attempts to make radiometric measurements on this program, some difficulty was encountered in obtaining a load material that was not reflective at the high frequencies of interest. This problem is severe in radiometry because of the extreme sensitivity of the receivers, since a small amount of local oscillator power at the signal frequency may leak out of the antenna, be reflected from the load, and self-mix in the mixer, causing problems with the detected signal. It is therefore very important to design radiometric loads for MMW applications which have very low reflectivity. Commercially

available sheet absorbing material, while adequate for the shorter microwave frequencies, has an unacceptably high reflectivity at higher frequencies. A solution to this problem was worked out at Georgia Tech which is also an important contribution to MMW technology made with support from this grant. Commercially available microwave absorbing epoxy was either machined or cast into a form consisting of linear rows of triangular cross section with the half-angles between rows chosen to be equal to Brewster's angle for the material, as shown in Figure 3-13. Radiation polarized perpendicular to the rows will then be transmitted into the epoxy where it is absorbed. It is also possible to make the loads insensitive to polarization by using both rows and columns with half-angles equal to Brewster's angle. These loads have been found to have extremely low reflectivity and have been extensively used in both calibration and reference applications in radiometers built at Georgia Tech.

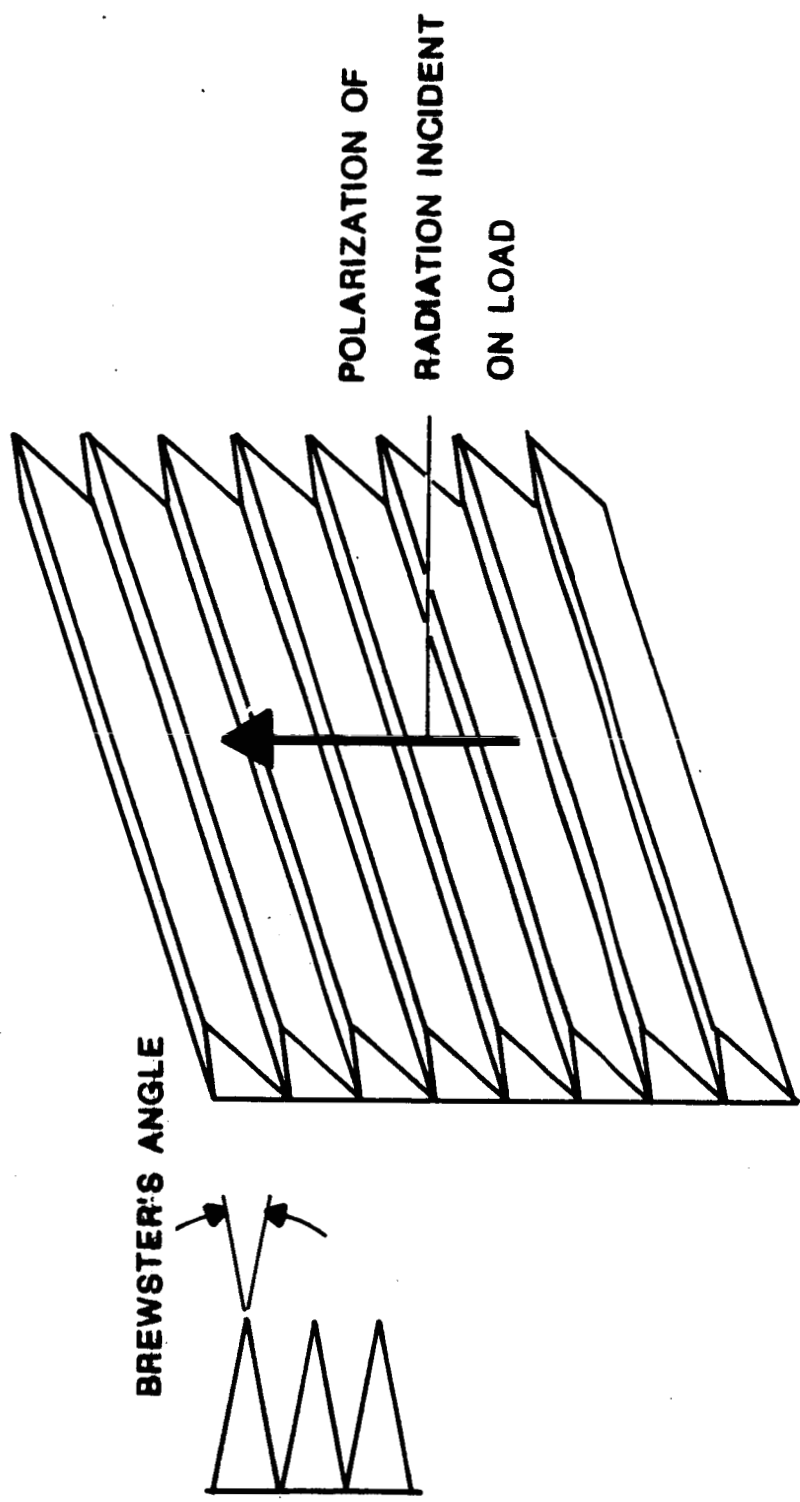


Figure 3-13. Diagram of radiometric load developed with support from this grant.

#### 4. Mixer Research

An area in which perhaps the most important contributions to MMW technology were made during the course of this grant is the area of MMW receiver mixer design and development. This area of research has also contributed greatly to other NASA programs at Georgia Tech, especially those involving the design and deployment of radiometers, and has made significant contributions to other MMW programs in GTRI. The most important of these non-NASA programs which benefited from mixer technology developed under NSG-5012 was a contract with the U. S. Army Night Vision and Electro-Optics Laboratory for the development of a 225 GHz radar system. One of the key elements in the design of this radar was the subharmonic mixer, basically developed during this grant, which gave state-of-the art performance and allowed for the implementation of an all solid-state receiver. Several other programs have also benefited from techniques developed for mixer design and fabrication during this grant, notably a program for the development of 94 and 140 GHz beamrider systems for the Army and a recently-funded Army effort for design, fabrication, and testing of a 340 GHz Sub-MMW imaging system.

Two types of mixers have been designed and utilized during this grant: (1) single-ended fundamental mixers which use a local oscillator near the signal frequency and a single point-contact diode as the active element, and (2) subharmonic mixers which use local oscillators at one-half or one-fourth the signal frequency and two back-to-back point-contact diodes. Each of these mixer types will be discussed in more detail in the following sections.

All of the diodes used in MMW research during the course of this grant were of the Schottky-barrier type. These diodes are fabricated by masking a piece of gallium arsenide with an array of holes on the order of only one micron in diameter. The GaAs is passivated everywhere except at the locations of these holes

with a layer of silicon oxide ( $\text{SiO}_2$ ), but the holes are filled with a layer of gold, thus forming a Schottky-barrier. The diode is formed by carefully contacting one of these holes with a metal whisker, generally made of gold-plated tungsten which has been bent to form a spring. This operation requires great care, because the contact pressure is extremely high, and the whisker is easily damaged. Figure 4-1 is an electron microscope photograph which shows a properly contacted diode of this type, and Figure 4-2 shows a poor diode in which the whisker was damaged by excessive pressure. Additional photographs in this section will show contacted diodes on a larger scale, and will indicate how the springs are fabricated and how the contact is made.

Schottky-barrier diodes have large forward resistances at low currents, so that it is difficult to self-bias them with LO power, especially at the higher MMW frequencies where LO power is scarce. For this reason, it is necessary to bias them with currents ranging from a few tens of microamperes to several milliamperes. To accomplish this biasing, several different circuits of different design have been fabricated, all of which use constant current sources and require careful shielding to avoid interference from local strong radio-frequency sources.

#### 4.1 Single-Ended Mixers

Before the development of the subharmonic mixers for the radiometers built for NASA for this grant and for subsequent programs, several different types of single-ended mixer were designed, fabricated and tested. These mixers were designed with guidance from Dr. G. T. Wrixon of University College in Cork, Ireland, who had been designing state-of-the-art MMW mixers for several years, and who served as a consultant to this program during 1975-1976. Dr. Wrixon also fabricated the diodes used in

ORIGINAL PAGE IS  
OF POOR QUALITY

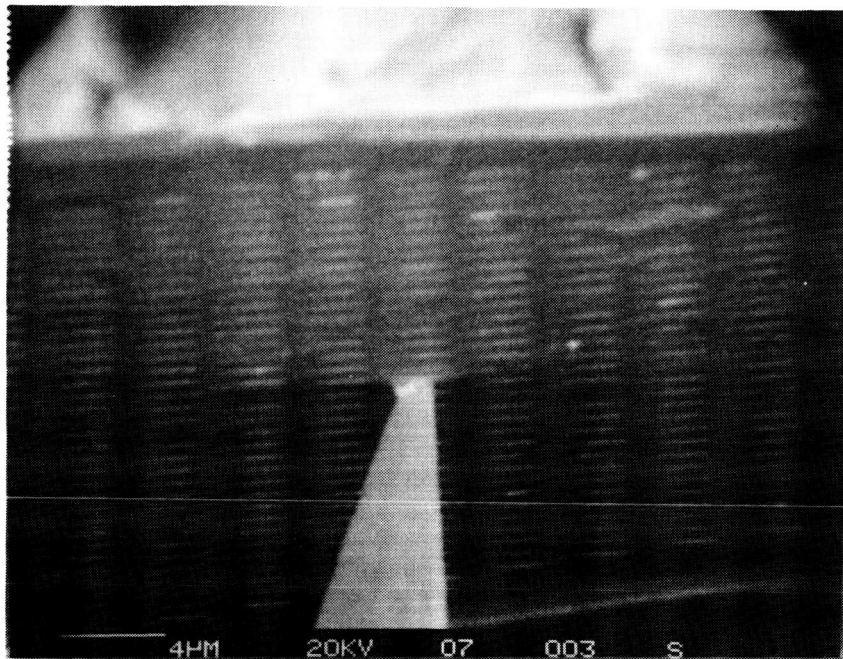


Figure 4-1. Scanning electron microscope photograph of whisker contacting a GaAs chip to form a diode. Note the array of holes as described in the text. The line at the lower left is a reference distance of 4 microns.

ORIGINAL PAGE IS  
OF POOR QUALITY



**Figure 4-2.** Scanning electron microscope photograph of a faulty diode contact showing a damaged whister. The line at the lower left is a reference distance of 1 micron.

the mixers fabricated on this program. Other diodes were furnished by Dr. Robert Mattauch of the University of Virginia through NASA Goddard.

#### 4.1.1 Sharpless Wafer Mixers

The earliest mixers built with support from this grant were of the Sharpless wafer type, which means that the diode was mounted in a so-called Sharpless wafer so that it could be easily contacted. In contacting a point-contact diode for MMW applications, it is important that the process be observable visually as well as with a curve tracer, so that the person performing the operation has some feel for the distance between the whisker and the diode chip. With the Sharpless wafer, which is a flat piece of gold-plated brass about 1 mm thick, the diode contacting process can be observed fairly easily, and after contact is made, the whole assembly is placed in the mixer body. Figure 4-3 is a sketch of a typical Sharpless wafer. The diode chip is soldered to a post, which is then pressed into the wafer through a hole lined with epoxy which acts as an insulator. The combination of the epoxy and the dimensions of the post determine an intermediate frequency (IF) filter which acts to match the diode to the IF amplifier input, for which the post serves as center pin, as shown in the sketch. A whisker is soldered to another post, and the diode is contacted by pressing this post into the Sharpless wafer body by means of a micrometer screw. As the screw is turned, the operation is observed through a microscope until the whisker is very close to the surface of the diode chip. The curve tracer is then observed at the same time to ensure that a good diode is formed by the contact. The shape of the diode curve on the curve tracer is an important indication of the performance of the diode when it is placed in a system. Sharpless wafer mixers were fabricated in both WR-10 (0.100 x

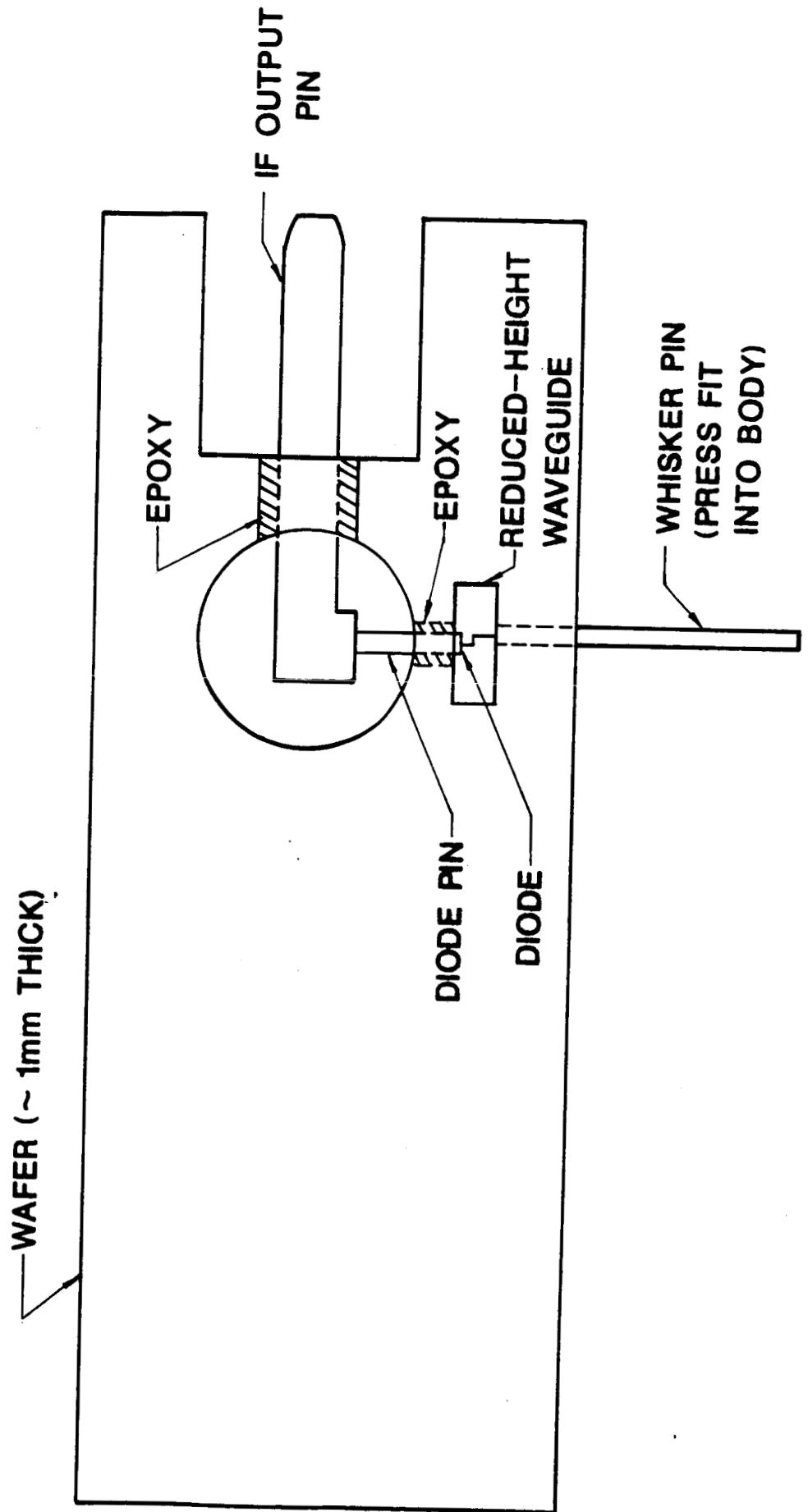


Figure 4-3. Sketch of a Sharpless wafer diode mount.

0.050 inches; 75-110 GHz) and in WR-5 (0.050 x 0.025 inches; 170-220 GHz) waveguides, because these bands were of interest for studying the 94 GHz atmospheric window and the 183 GHz water vapor transition during the course of this program. Double-sideband noise figures of about 6 and 10 dB, respectively, were obtained at these two frequencies using these Sharpless wafer mixers.

#### 4.1.2 Split-Block Mixer

Before the design and fabrication of the subharmonic mixers had matured sufficiently so that this technology could be used in radiometer systems, a different type of single-ended mixer called a split-block mixer was designed and built for this program. This mixer was large and heavy, and was designed to be mechanically rugged for good stability in maintaining contact of the diode. Figure 4-4 is a diagram of this mixer, showing the locations of the diode chip, whisker, IF filter, and backshort. The name "split-block" refers to the method of fabrication of this device, since the waveguide channels had to be machined into the brass mixer body before assembly. After machining and polishing, the mixer was gold plated, and was then carefully assembled using stainless steel locator pins for proper alignment. Unlike the Sharpless-wafer mixer, it was not possible to contact this device before assembly. To visually observe the contacting process for this mixer, a microscope was used to look down into the waveguide with back-lighting from a microscope lamp shining into the backshort waveguide port. Because of the necessity for contacting in this way, the split-block mixer was more difficult to contact than the Sharpless-wafer type. The split-block mixer was used in radiometers built for the earliest Convair 990 flights on which MMW radiometers were flown, and achieved a double-sideband noise figure of 7 dB for an IF of 1 GHz.

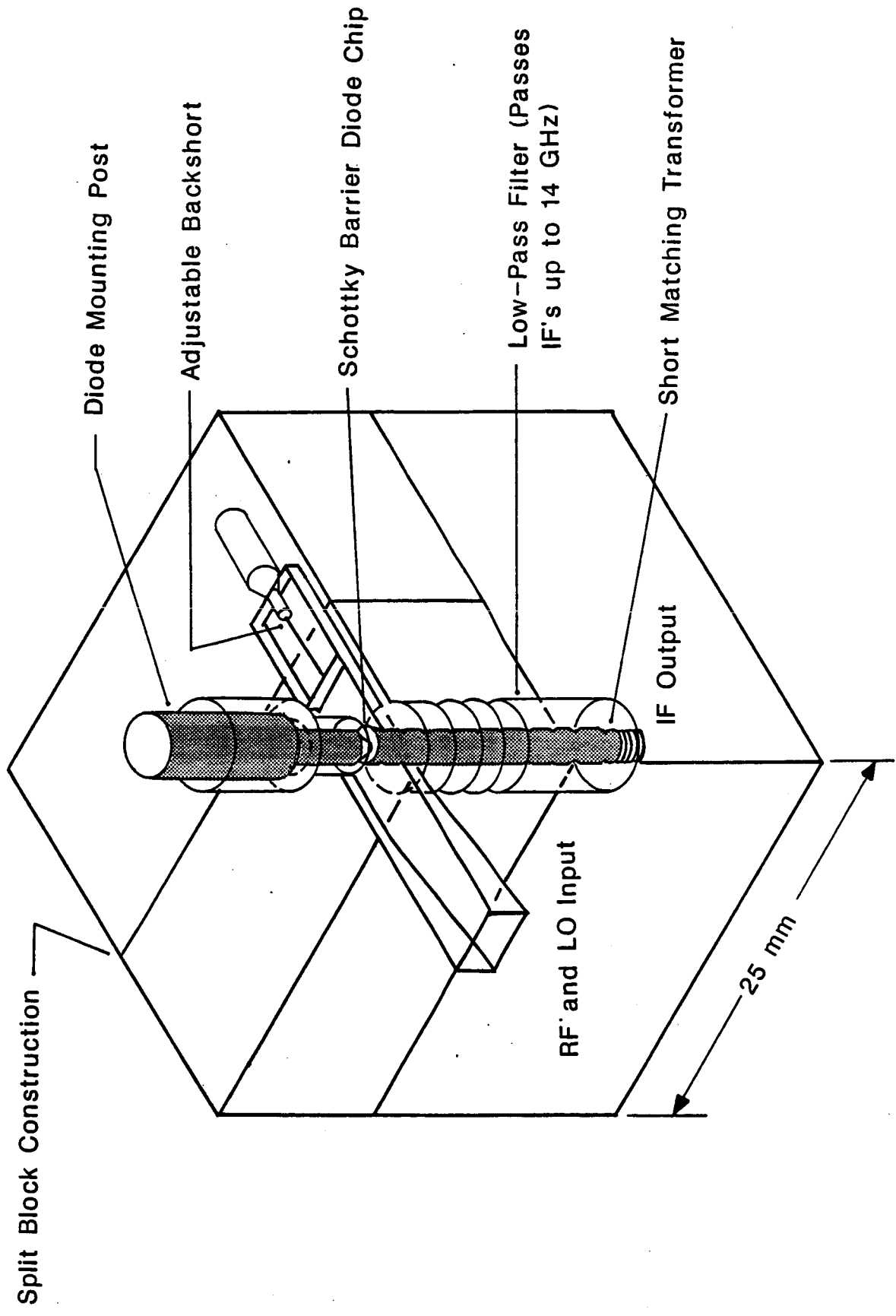


Figure 4-4. Diagram of the split-block single-ended 183 GHz mixer used for early Convair 990 flights as described in the text.

#### 4.1.3 Diplexers for Single-Ended Mixers

At the time that the work on single-ended mixers discussed above was being done, the design of suitable diplexers for coupling both LO and signal power into the mixer through a single waveguide was a significant problem, and for single-ended mixers, this problem still exists. The earlier crossguide harmonic mixers did not suffer from these limitations because waveguide ports were provided for both signal and LO, but these devices did have limitations on performance set by the necessity for multiplying the LO frequency in the mixer diode and by the length of the whisker, which had to traverse both waveguides. Likewise, recently-designed double-balanced and subharmonic mixers have separate waveguide ports, and do not suffer from the limitations imposed on either the single-ended mixers or the cross-guide mixers, but these devices were not available early in the grant. Indeed, significant contributions to the development of subharmonic mixers were made during the course of this grant, as will be discussed in the next section.

Methods for diplexing signal and LO at lower frequencies require the use of directional couplers, circulators, or hybrid rings. Directional couplers are useful diplexers in applications where plentiful LO power is available, but at the higher frequencies, LO power is generally scarce, and the losses imposed by directional couplers for both signal and LO paths cannot be tolerated. Circulators with tolerable losses are not available at frequencies much above 100 GHz, and it is possible to design diplexers by other methods which outperform these devices. Hybrid rings or "rat-races," or other such devices are difficult to fabricate in the smaller waveguide sizes required for the higher frequencies.

To avoid these problems, the single-ended mixers designed

early in the term of this grant were based on resonant-cavity couplers, as shown in Figure 4-5. The signal power passed directly into the mixer through the waveguide, but LO power was coupled in through a fundamental-mode resonant cavity which was carefully machined to pass the LO frequency. Fine-tuning of the cavity resonance was accomplished by slightly changing the cavity size with sandpaper, and by adjusting the mounting screws to bear in slightly different ways on the cavity. Unwanted modes were eliminated by properly choosing the locations of the input and output coupling holes, as well as the cavity size. These operations were monitored by placing a signal into the LO port and maximizing it at the mixer port, and by repeating this process for the signal port to ensure that signal power did not pass into the LO input port. This process was iterated until losses at LO and signal ports were minimized. At first, it was necessary to make these measurements using reflex klystron oscillators, intended for LO applications, for both signal and LO sources, but they were later made with wideband sweepers based on tunable IMPATT diode oscillators.

These cavity couplers worked very well at 94 GHz, where LO port losses were about 3dB and signal port losses were less than 1 dB. Also, the LO power available was on the order of tens of milliwatts, so that LO losses were inconsequential; however, at 183 GHz, a frequency of greater interest to NASA, the performance of these couplers was not as good. For this frequency, they were used with a reflex klystron oscillator and a doubler acquired from Airborne Instruments Laboratory, to be described later. In this application, the cavity diplexers had a loss in the LO port of 6-7 dB and a signal-port loss of about 1 dB. Using the klystron-doubler combination, this performance was adequate, although it was always necessary to bias the mixer diodes for optimum performance. This LO configuration was used in the 183

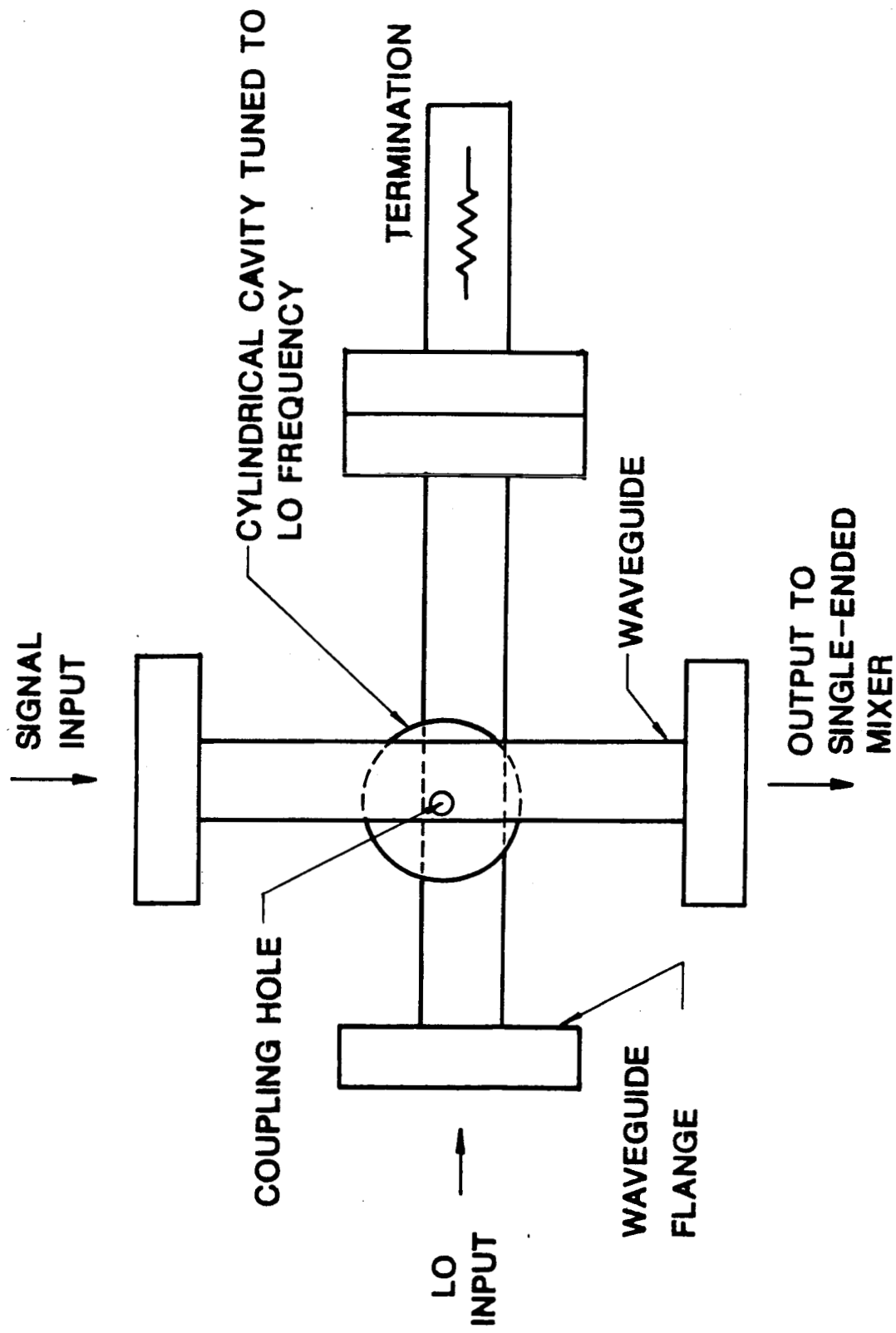


Figure 4-5. A resonant cavity coupler used for diplexing signal and L.O.

GHz radiometer for the early Convair 990 flights, but the coupling-cavity diplexers were never very stable, especially at the higher frequencies. An advantage of these cavity diplexers not mentioned above is that they tend to provide some measure of filtering of the LO signal, so that LO power at the signal frequency is rejected to some extent. Since all sources of radiation, even though they may be phase locked, do have very wide bandwidths over which infinitesimal amounts of power are radiated, this filtering capability is an important feature of the cavity diplexer; however, it is a feature that is shared by most well-designed diplexers.

To avoid these fabrication and mechanical stability problems, a quasi-optical diplexer, first proposed by Gustincic [17] was studied in some detail. These studies are the basis for the detailed calculations of the transmission and reflection properties of arrays of wire grids presented in Section 5. These calculations showed not only that it is possible to make diplexers from wire grids, but that it is also possible to do a number of other operations, including the fabrication of tunable bandpass and band-reject filters, as discussed in Section 5.

Figure 4-6 is a schematic diagram of the diplexer proposed by Gustincic. Signal power, polarized parallel to the page, is incident from the left, and passes through the four-grid Fabry-Perot interferometer, which is tuned to pass this signal frequency. This signal then passes through the  $45^\circ$  wire grid, which has its wires oriented perpendicular to the page, and is focused into the mixer by the lens, as shown. Local oscillator power, polarized perpendicular to the page, is incident from below, and is reflected from the  $45^\circ$  grid into the interferometer, where it is reflected from the interferometer with an accompanying polarization rotation of  $90^\circ$ , passes through the  $45^\circ$  grid, and from thence into the mixer, where it is mixed with the signal to give the IF.

Because the subharmonic mixers to be described in the next

POLARIZATION-TWISTING  
FOUR-GRID FABRY-PEROT INTERFEROMETER  
TUNED TO SIGNAL FREQUENCY

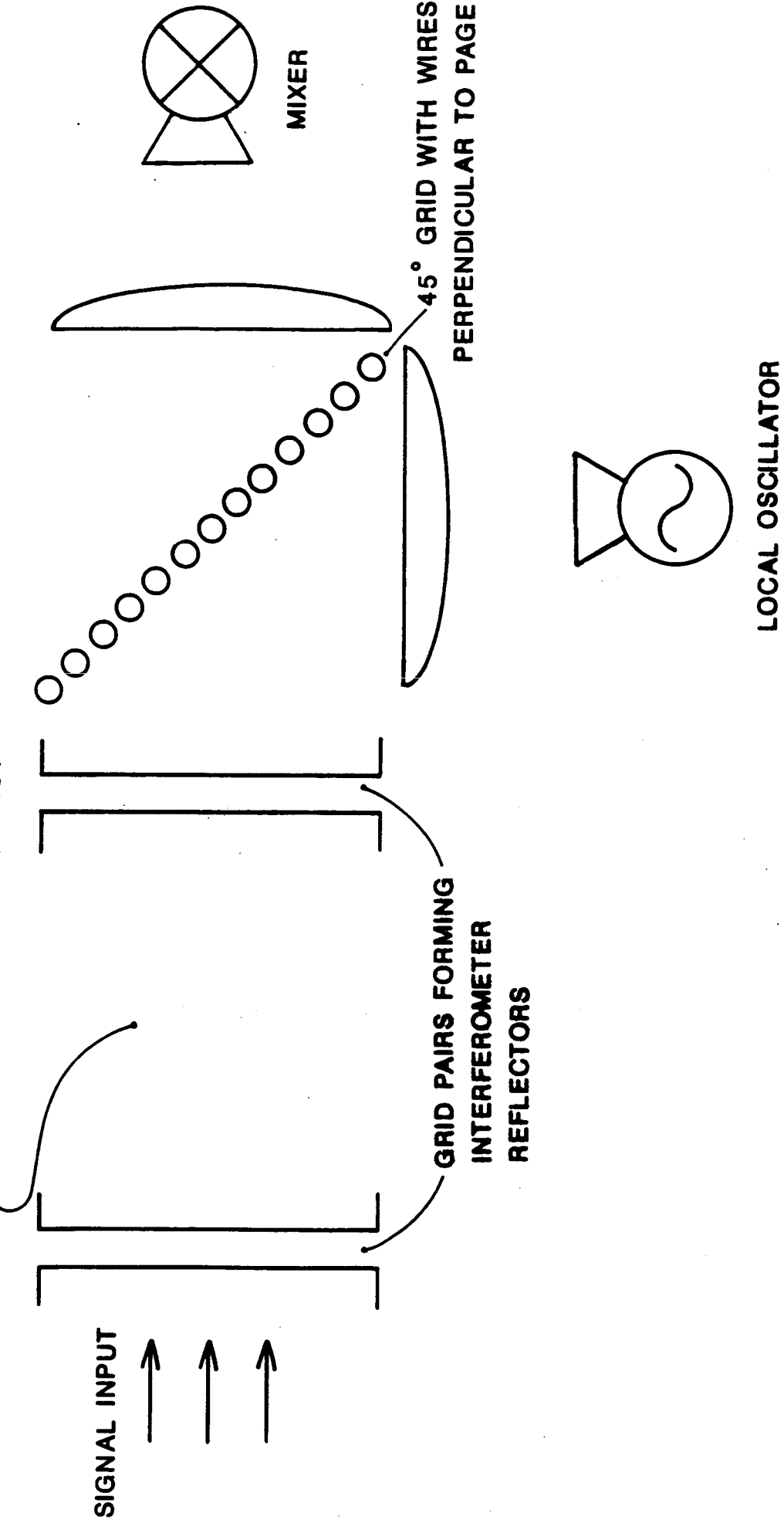


Figure 4-6. Schematic diagram of the Gustincic diplexer made of two pairs of wire grids forming an interferometer.

section were shown to have excellent performance capabilities at 183 GHz, and these devices do not require a diplexer, the quasi-optical diplexer described above was never built, although several grid array interferometers were constructed and tested to verify the equations derived in Section 5. One of the results of these equations is that it is not possible to build a four-grid interferometer with the configuration shown that rotates the plane of polarization of incident radiation on transmission, but that rotation can be achieved on reflection with a two-grid array. Based on Gustincic's presentation at Georgia Tech in early 1976, it was understood that this polarization rotation was accomplished on transmission, but this difference is of little consequence, since LO and signal inputs can be interchanged in any case, with appropriate tuning. This latter configuration might actually be preferable, since the signal would not be subjected to the losses inherent in a high-finesse interferometer tuned to its signal frequency.

#### 4.1.4 Local Oscillator Doublers for Single-Ended, Fundamental Mixers

When single-ended mixers were being built for 183 GHz operation in the early days of this grant, no suitable fundamental local oscillator sources were available. Although klystron oscillators could be built at this frequency, they were expensive and unreliable. IMPATT sources were also available at 183 GHz, but were considered too noisy for local oscillator applications, although the capability to phase lock these sources, developed during the past few years, has made them attractive as local oscillators. This problem was solved early in the course of this grant by having an efficient doubler developed for 91.5 - 183 GHz by Airborne Instruments Laboratory. At the time this doubler was developed, it was possible to purchase a klystron oscillator from Varian Associates capable of an output power in excess of 100 mW at 91.5 GHz, an amount considered sufficient to drive a doubler to an output of perhaps 10 mW output at 183 GHz. Figure 4-7 is a photograph of the doubler designed and built for this grant by AIL. This device used varactor diodes and carefully designed tuning circuitry to achieve high doubling efficiency; the device shown had an efficiency of 15 per cent for 100 mW input at 91.5 GHz. Considering a loss of perhaps 6 dB in a coupling cavity, this 15 mW at 183 GHz was adequate LO power for single-ended mixer applications, in which the diodes could be biased. This doubler was used in combination with the split-block mixer discussed above in the window-mount radiometer on some of the early Convair 990 flights.

#### 4.2 Subharmonic Mixers

It was mentioned earlier that the development of subharmonic mixers during the term of this grant is perhaps the most important contribution of this grant to MMW technology, having benefited other NASA programs at Georgia Tech as well as programs

ORIGINAL PAGE IS  
OF POOR QUALITY

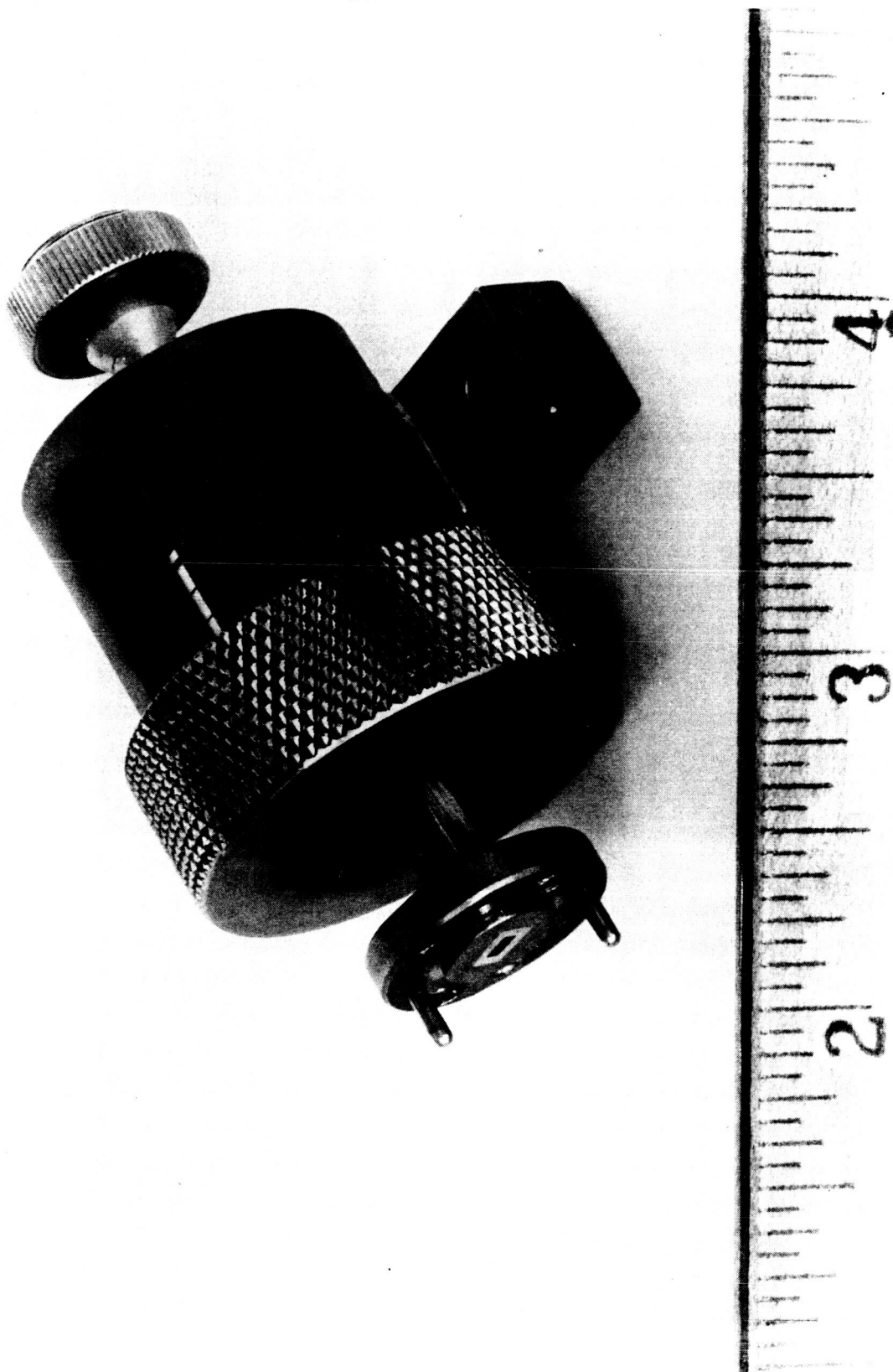
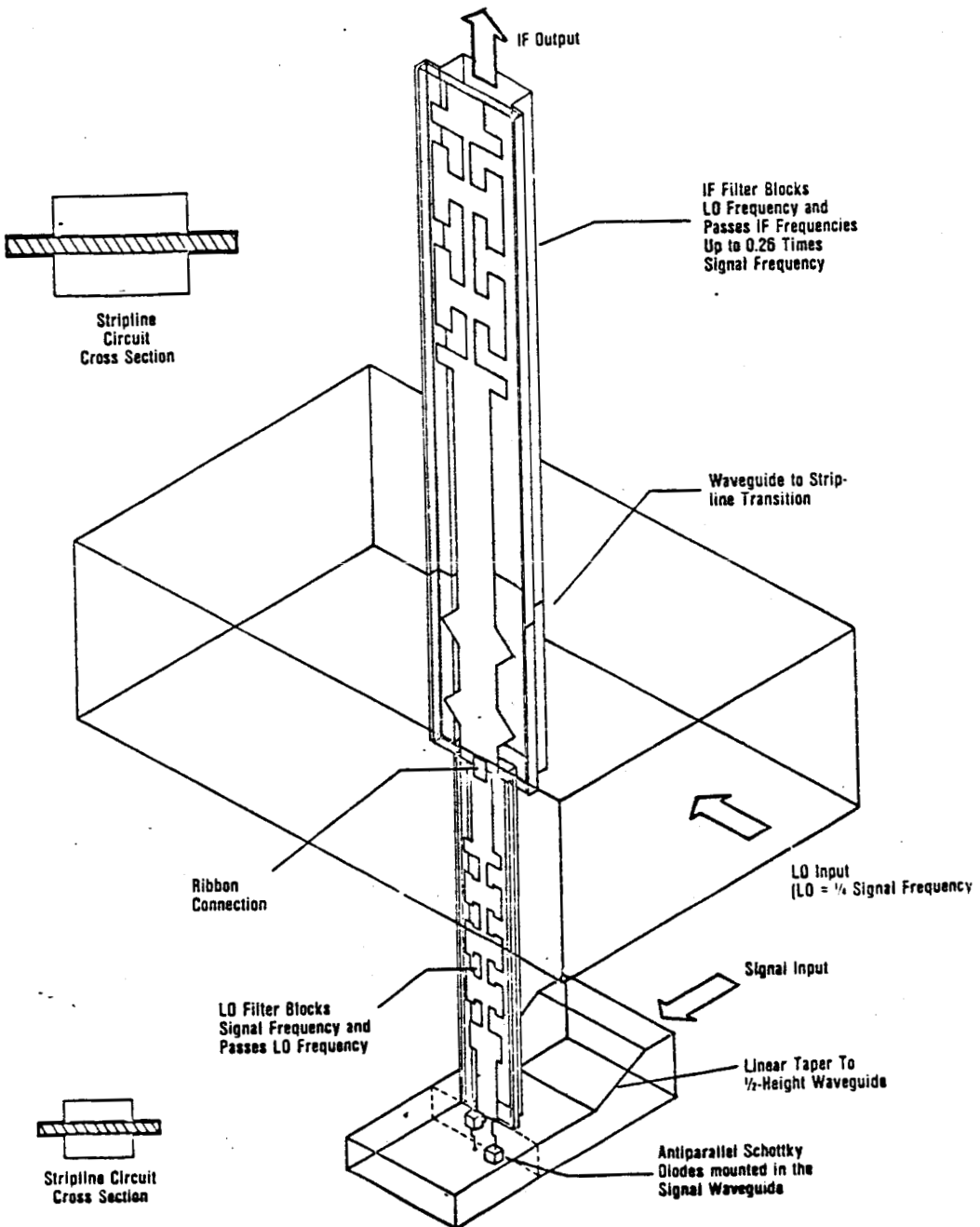


Figure 4-7. Photograph of the 91.5/183 GHz doubler designed and built by AII for this project.

for other sponsors. This section gives a brief discussion of how these mixers are designed and built and details the performance levels achieved with them [18].

In designing devices for the higher MMW frequencies, the degree of precision required dictates that the device first be modeled at some convenient lower frequency, because it is not generally possible to choose all dimensions for optimum performance when considering the small sizes of the final components. In designing subharmonic mixers for the WR-5 waveguide band, models were first constructed with fundamental frequencies in S-band (6 GHz). For the f/2 subharmonic mixers built for airborne radiometers on this grant, a 3 GHz local oscillator was then required, but for an f/4 device designed later with support from this grant, the model was modified to accommodate a 1.5 GHz LO. Since the final mixer was required to operate with waveguide signal and LO inputs, it was necessary to fabricate waveguides for these lower frequencies, because waveguides for these bands are not available commercially. For the case of the 1.5 GHz LO, the waveguide was more than 20 cm wide by 10 cm high.

Figure 4-8 is a schematic diagram of the f/2 mixer built on this grant. The heart of this mixer is a quartz stripline circuit comprising several filters which separate input, LO and IF signals. The lower filter blocks the input signal from passing up the stripline while passing the LO signal to the diodes and IF power to the IF output. The upper filter blocks LO signal from the IF port, while passing the IF signal. It is possible to fabricate these filters on stripline such that the mixer has a very broad bandwidth, which was a requirement for profiling the water vapor transition for the 183 GHz radiometers for which this mixer was designed. Power input to the LO port is optimized by the LO backshort and collected by the stripline where it is directed to the back-to-back diode pair in the signal waveguide. The diodes produce only even harmonics of the LO, and



**Figure 4-8.** Schematic diagram of the subharmonic mixer designed and built with support from this grant. Both  $f/2$  and  $f/4$  versions of this mixer were built.

suppress the fundamental, so that the signal incident into the signal waveguide mixes with the second harmonic of the signal frequency to generate the IF, which passes through the stripline to the IF output port. Signal input is also optimized by a backshort, and the waveguide tapers to half-height to better match the waveguide impedance to the diodes.

In modeling this device, the mixer body is machined from aluminum in halves, so that channels for the stripline and waveguides may be cut on a milling machine. A similar procedure is followed when fabricating the final 183 GHz device. Stainless steel locator pins serve to give good mixer body alignment and maintain this alignment. The stripline circuit is fabricated by placing copper tape on a piece of quartz approximately 25 mm wide by 20 cm long by 2 mm thick. In this way it is easy to tailor the circuit to give the desired performance by simply trimming the circuit with a razor blade; or it is easy to simply start over by stripping the copper tape from the quartz. A preliminary design was formulated by analysis, and the arrangement of the tape on the quartz was made accordingly. The circuit was then tested using equipment readily available for this low-frequency band, such as sweep generators and spectrum analyzers, so that an optimum configuration was obtained. The stripline circuit was then scaled down in size by a factor of about 30 for the 183 GHz mixer. Note that it would have been almost impossible to design the tiny stripline circuits without beginning with the model, because the final devices are less than one cm in length and one mm in width.

Besides the mixer body and the stripline, it was also necessary to scale the mixer diodes. At 6 GHz, packaged high-performance Schottky-barrier diodes are available commercially, but the diode chips that are available at 183 GHz must of course be contacted. Also, the 183 GHz diodes are roughly 0.25 mm square by 0.15 mm thick, and therefore take up a significant portion of the half-height 1.2 X 0.3 mm waveguide in which they

are mounted. The 6 GHz diodes are much smaller than the 6 GHz waveguide in the model, so that it was necessary to somehow simulate this great size differential in the model. This simulation was accomplished by mounting the 6 GHz diodes on brass blocks scaled to cover the same proportion of the model waveguide volume as the GaAs diodes occupy in the final 183 GHz version of the mixer. This approach of course compromised the performance of the mixer model, but gave such an accurate preview of the final mixer performance that the 6 and 183 GHz versions of the mixer differed only by about 1 dB in noise figure performance.

Figure 4-9 is a photograph of an f/2 subharmonic mixer built for 183 GHz. The micrometer screws are used for tuning the signal and LO backshorts. Figure 4-10 is a photograph of the disassembled mixer showing the stripline channel. This mixer must be fully assembled before contacting because assembly after contacting requires tightening screws which invariably place enough strain on the structure to cause the diodes to lose contact. In contacting this mixer, one diode chip and one whisker are each soldered to the stripline circuit, and a diode chip and a whisker are each soldered to separate pins. The whisker pin is then pressed into the mixer body to contact the diode on the stripline, and the diode pin is pressed into the body to contact the whisker, thus forming the back-to-back diode combination required for this mixer. Since this mixer must be contacted while assembled, it is necessary to observe the contacting process through the waveguide, with illumination through the backshort port. Figure 4-11 is a photograph of mixer diodes contacted in this way, showing the two diode chips, whisker springs, and the bottom edge of the stripline circuit. This photograph emphasizes the small size of the signal waveguide and the other components, and shows why it was necessary to model the diode chips at 6 GHz with brass blocks.

It was mentioned earlier in this section that Schottky-barrier diodes generally require bias for optimum performance.

ORIGINAL PAGE IS  
OF POOR QUALITY

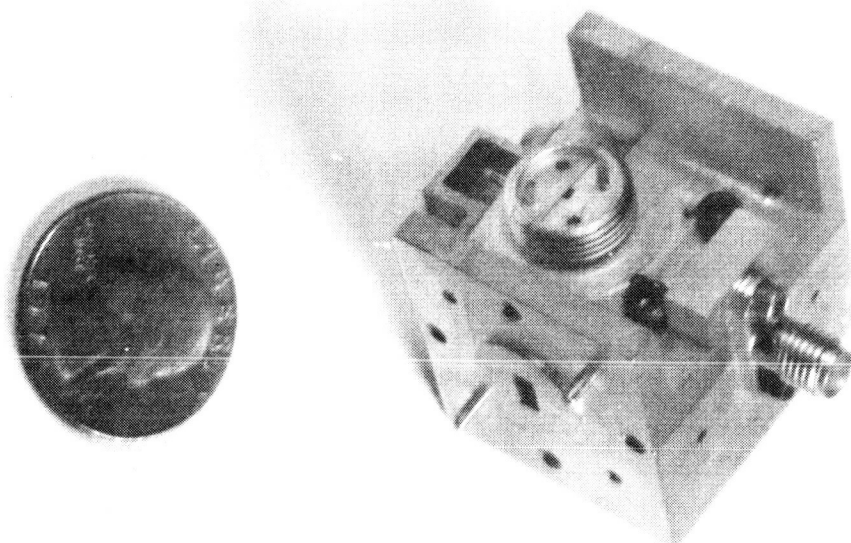


Figure 4-9. Photograph of assembled f/2 subharmonic mixer. The signal port is at top, the LO port is below, and the IF output is to the right.

ORIGINAL PAGE IS  
OF POOR QUALITY

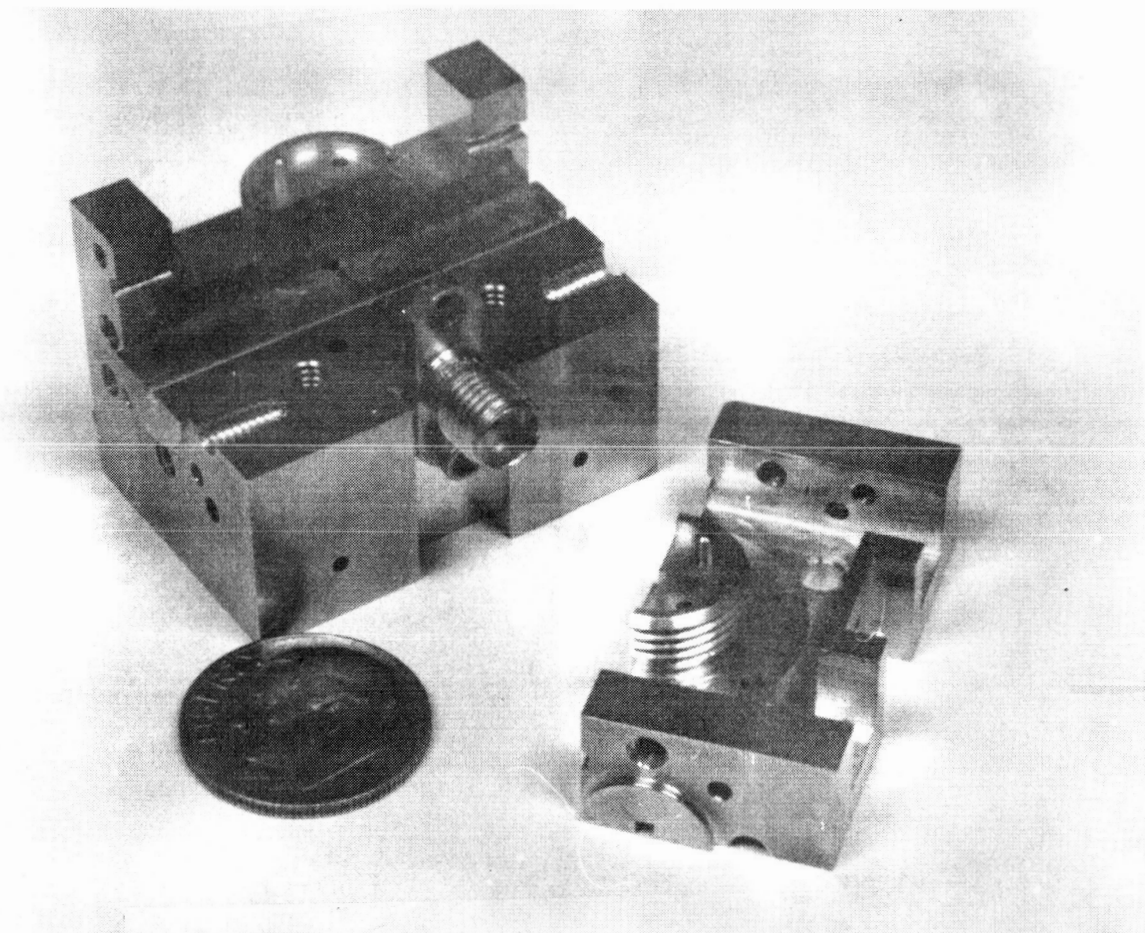


Figure 4-10. Photograph of f/2 mixer disassembled to show stripline channel immediately below IF port.

ORIGINAL PAGE IS  
OF POOR QUALITY

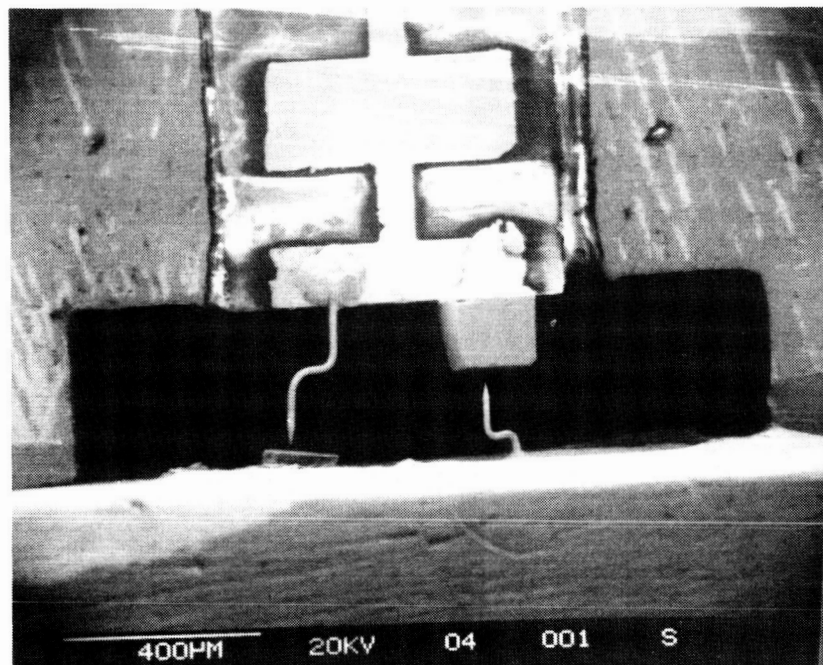


Figure 4-11. Scanning electron microscope photograph of diode and whisker mounted to stripline. A diode and a whisker are pushed up from below to contact the mixer as shown.

Unfortunately, a method of supplying bias current to the subharmonic mixer has not yet been devised, so that the mixer diodes must be biased into their proper operating range by LO power. This method of biasing the subharmonic mixers is costly in LO power to the extent that perhaps an order of magnitude more LO power is required for the subharmonic mixer than for biased single-ended devices. This requirement does not generally impose limitations because adequate power is usually available at one-half the signal frequency. An exception to this statement occurs when one wishes to extend operation to 225 GHz and wishes to build an all solid-state receiver. The maximum frequency of operation of GaAs Gunn oscillators is about 100 GHz, and IMPATT oscillators, which are available in this frequency range, are generally considered too noisy for LO applications. This problem may be solved by choosing the f/4 mode of operation, which requires a Gunn oscillator operating at about 55 GHz, a frequency at which adequate power is available for pumping a subharmonic mixer. It is thus possible to achieve the desired output from a source quiet enough for local oscillator applications, and still retain the advantages of all solid-state operation.

The mixer shown in Figure 4-8 gave a double-sideband noise figure of 4.9 dB at 183 GHz at an IF of 1 GHz, a performance level that remains essentially state-of-the-art some eight years after it was achieved. Noise figures obtained at IFs of 5 and 10 GHz with this mixer were 5.9 and 7.9 dB, respectively. A comparable mixer designed for f/4 operation at 225 GHz in an Army radar system gave a DSB noise figure of 8.5 dB with an IF of 750 MHz.

## 5. Properties of Wire Grid Arrays (20)

### 5.1 Calculations of Transmission and Reflection

The properties of wire grid arrays were of interest to NASA and Georgia Tech because of their potential usefulness as diplexers for combining LO and signal into a single mixer. The development of subharmonic mixers, discussed in the last section, eased the requirement for these devices to some extent, especially for applications related to this grant, but diplexers are still needed for many high-frequency applications, beyond the capability of subharmonic mixers. Because of their low loss and ease of fabrication, optical diplexers are especially useful for these high frequency applications; however, no wire-grid or other optical diplexers were fabricated with support from this grant because the requirements were obviated by the availability of excellent subharmonic mixers.

Although diplexers were not fabricated, analysis of the wire grid arrays which were to serve as building blocks for them revealed a variety of very interesting properties of these devices that indicate that they may be very useful in MMW and sub-MMW systems, especially at the higher frequencies. Some of the possible applications of these arrays include tunable bandpass and band-reject filters, polarization rotators, and simple polarizers. This section treats the analysis of these devices and the next section compares these calculations to experiment.

In analyzing the properties of wire grid arrays the configuration shown in Figure 5-1 was used for each grid pair. One grid is oriented at an angle  $\theta$ , and the second is oriented at angle  $\alpha$ . The phase shift between these grids is taken to be  $\phi$ , and the polarization angle of the input radiation is denoted by the angle  $\beta$ , measured relative to the horizontal. Unfortunately, when these calculations were made, the convention was chosen so that the angles indicated are measured perpendicular to the grid

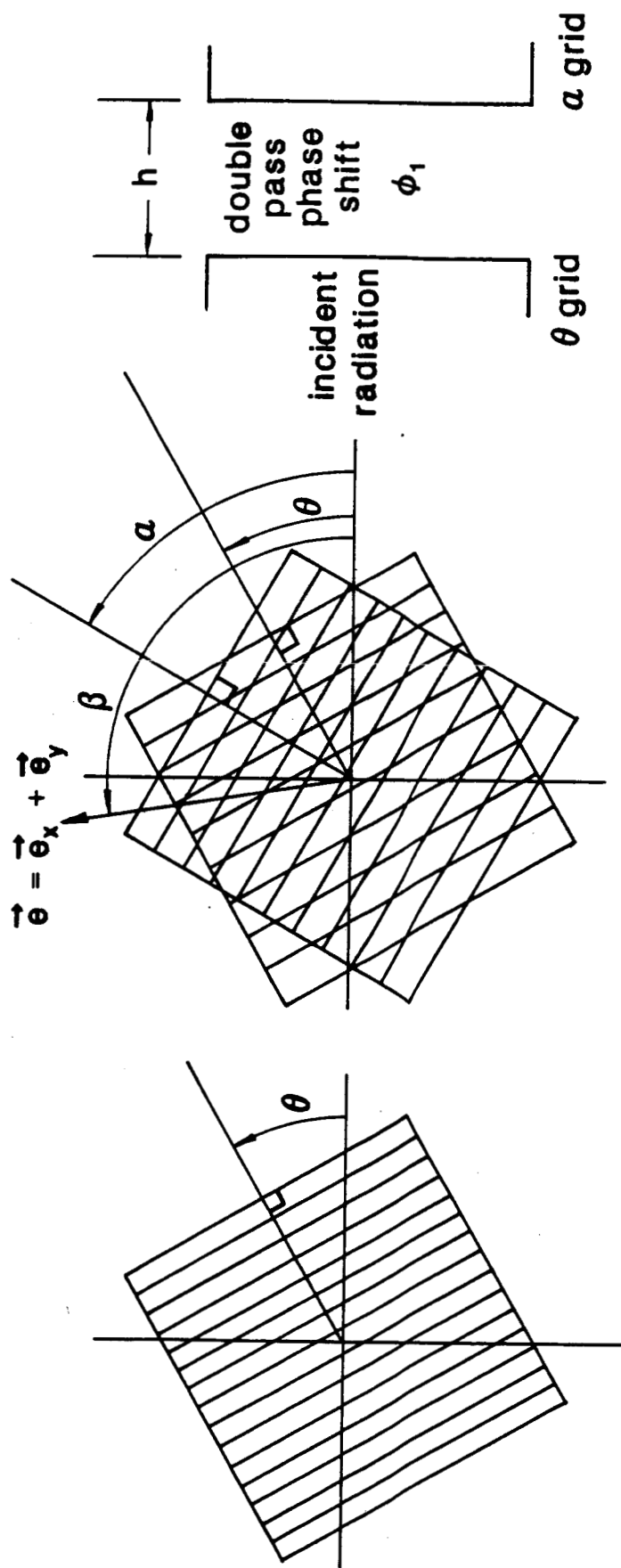


Figure 5-1. Diagram showing the conventions chosen for orientation of grid wires.

wires, instead of parallel to them, a choice that may lead to some confusion unless one is careful. A four-grid array is formed by choosing two pairs of grids as shown in Figure 5-1 and separating them by a phase shift  $\phi_3$ . The angle between the grids is designated  $\gamma$ . The derivations to be discussed in this section are quite general in that arbitrary grid angles and phase shifts may be chosen, so that the angles for the second pair of grids are  $\theta_2$  and  $\alpha_2$ ; however, the most interesting properties of these devices become evident when the configuration is symmetrical, i.e. when  $\theta_1 = \theta_2$  and  $\alpha_1 = \alpha_2$ .

All of the calculations described in this section were made under the assumption that, except for losses, radiation polarized parallel to the grids is totally reflected and that polarized perpendicular to the wires is totally transmitted. This means that the grids are perfect polarizers, again excepting losses. Losses are accounted for by using transmission factors  $T$  and reflection factors  $R$  which modify the transmission and reflection terms.

A brief synopsis of the procedure used in deriving the general equation for four-grid interferometer amplitude transmission will be given. In deriving this type equation, one obtains an infinite series because of the hierarchy of reflections and transmissions that occur at each grid. If possible it is very useful to be able to write this series in the form

$$1 + X + X^2 + \dots + X^n + \dots = \frac{1}{T-X}, \quad (5-1)$$

because of the very simple nature of the closed form solution. This procedure is used by Born and Wolf [19] in deriving the expression for transmission of a Fabry-Perot Interferometer (FPI) using plane partial reflectors.

Upon taking this approach, the amplitude transmission  $A_{TF}$  for the four-grid FPI has been determined to be

$$\vec{A}_{TF} = T^2 e^{i\delta} R_1 R_2 \cos\gamma_1 \cos\gamma_2 \cos A M_1 \left\{ 1 + e^{2i\phi_3} (M_2 - T_1 M_3) (M_4 - T_2 M_5) \right. \\ \left. + e^{4i\phi_3} [(M_2 - T_1 M_3)(M_4 - T_2 M_5)]^2 + \dots \right\} M_6 \begin{pmatrix} e_x \\ e_y \end{pmatrix}, \quad (5-2)$$

where:

$T$  = transmission of a single grid with input radiation polarized perpendicular to its wires,

$R_1$  =  $\phi_1 + \phi_2 + \phi_3$ , and the  $\phi$ 's are phase shifts between individual grids,

$$R_1 = \frac{1 - Re^{2i\phi_1}}{1 - Re^{2i\phi_1} \cos^2 \gamma_1}, \quad R_2 = \text{same with sub-1's replaced by sub-2's},$$

$$T_1 = \frac{Te^{2i\phi_1} \sin^2 \gamma_1}{1 - Re^{2i\phi_1} \cos^2 \gamma_1}, \quad T_2 = \text{same with sub-1's replaced by sub-2's},$$

$R$  = reflection of a single grid with input radiation polarized parallel to its wires,

$\gamma_1 = \theta_1 - \alpha_1$ ,  $\gamma_2 = \theta_2 - \alpha_2$  in which the  $\theta$ 's and  $\alpha$ 's are individual grid angles,

$A = \alpha_1 - \alpha_2$ .

The M's are  $2 \times 2$  products of transmission and reflection matrices for individual grids and are given by

$$M_1 = \begin{pmatrix} \cos\theta_2 \cos\alpha_2 & \cos\theta_2 \sin\alpha_2 \\ \sin\theta_2 \cos\alpha_2 & \sin\theta_2 \sin\alpha_2 \end{pmatrix}, \quad M_2 = \begin{pmatrix} -\sin^2\alpha_1 & \sin\alpha_1 \cos\alpha_1 \\ \cos\alpha_1 \sin\alpha_1 & -\cos^2\alpha_1 \end{pmatrix}$$

$$M_3 = \begin{pmatrix} \cos^2\alpha_1 & \cos\alpha_1 \sin\alpha_1 \\ \cos\alpha_1 \sin\alpha_1 & \sin^2\alpha_1 \end{pmatrix}, \quad M_4 = \begin{pmatrix} -\sin^2\alpha_2 & \sin\alpha_2 \cos\alpha_2 \\ \cos\alpha_2 \sin\alpha_2 & -\cos^2\alpha_2 \end{pmatrix},$$

$$M_5 = \begin{pmatrix} \cos^2\alpha_2 & \cos\alpha_2 \sin\alpha_2 \\ \cos\alpha_2 \sin\alpha_2 & \sin^2\alpha_2 \end{pmatrix} \quad M_6 = \begin{pmatrix} \cos\alpha_1 \cos\theta_1 & \cos\alpha_1 \sin\theta_1 \\ \sin\alpha_1 \cos\theta_1 & \sin\alpha_1 \sin\theta_1 \end{pmatrix}.$$

Finally, the column vector matrix  $\begin{pmatrix} e_x \\ e_y \end{pmatrix}$  represents the input polarization and amplitude. Upon taking the approach suggested by Equation (5-1), the transmission becomes:

$$\vec{A}_{TF} = T^2 e^{i\delta} R_1 R_2 \cos\gamma_1 \cos\gamma_2 \cos\alpha$$

$$\cdot M_1 \left[ \frac{1}{1 - e^{2i\phi_3} (M_2 - T_1 M_3) (M_4 - T_2 M_5)} \right] M_6 \begin{pmatrix} e_x \\ e_y \end{pmatrix} .$$

(5-3)

Now consider only the terms involving the M's. Note that the bracketed term is itself a matrix, and if the inverse of its denominator exists, it will be possible to calculate  $A_{TF}$  by this method. The inverse  $M^{-1}$  of a matrix M is given by

$$M^{-1} = \frac{\text{adj } M}{|M|}, \quad (5-4)$$

where adj stands for adjoint and the denominator is the determinant of M. Note that none of the matrices  $M_1 - M_6$  have inverses that do not exist because each of their determinants is zero, but the matrix represented by the denominator of Equation (3) may well have an inverse because it is a combination of the transmission matrices with scalar terms. Fortunately, this turns out to be the case. Upon carrying out the indicated operations, the matrix part of Equation (3) becomes

$$\frac{1 - \text{Re}^{2i\phi_3} [1 + \sin^2 A(1 - T_1)(1 - T_2)] \cos A}{(1 - RT_1 e^{2i\phi_3})(1 - RT_2 e^{2i\phi_3}) - R \cos^2 A e^{2i\phi_3}(1 - T_1)(1 - T_2)} \cdot \begin{pmatrix} \cos \theta_1 \cos \theta_2 & \sin \theta_1 \cos \theta_2 \\ \cos \theta_1 \sin \theta_2 & \sin \theta_1 \sin \theta_2 \end{pmatrix}. \quad (5-5)$$

The power transmission as a function of frequency for an array of wire grids is of course the parameter of primary interest to the system designer. This transmission is given by the product of the amplitude transmission matrix with its complex conjugate,  $A P v T F * A^{TF}$ , where the asterisk denotes the complex conjugate. This product has been calculated for arbitrary values of all parameters including losses in the wire grids, and the

results will be compared to experiment in the next subsection. This equation for grid transmission is considered too lengthy for inclusion in this report, but is available from the author to anyone interested.

The fairly simple form of Equation (3) actually hides a very complicated result. If the expression (5) together with the expressions for  $R_1$ ,  $R_2$ ,  $T_1$ ,  $T_2$  are substituted into (3) the result is almost intractable when attempts are made to find the asterisk denotes the complex conjugate. For this reason, it has not yet been possible to derive this expression except for the special case mentioned above. The matrix part of the expression (5) will give polarization twisting on transmission for the proper choice of  $\theta_1$  and  $\theta_2$ , but it has been found that the balance of the expression goes to zero for all such choices of grid angle tried thus far.

## 5.2 Measurements and Calculations of the Properties of Wire Grid Arrays

The equations of Section 5-1 have been compared to experiments and found to give excellent agreement. Figure 5-2 shows calculated and measured transmission of a four-grid array at 70 GHz under the conditions specified on the figure. Note that this result is not for relative transmission; the equations accurately predicted the absolute transmission of the array by considering the losses in the wires. Several other examples of accurate prediction of array performance were observed during this series of measurements, both at 50 and 70 GHz, giving some confidence that the properties of these devices, as predicted by theory, will be useful in several MMW and sub-MMW applications. Several examples of these properties are discussed in the next few paragraphs.

One of the most interesting and potentially useful features

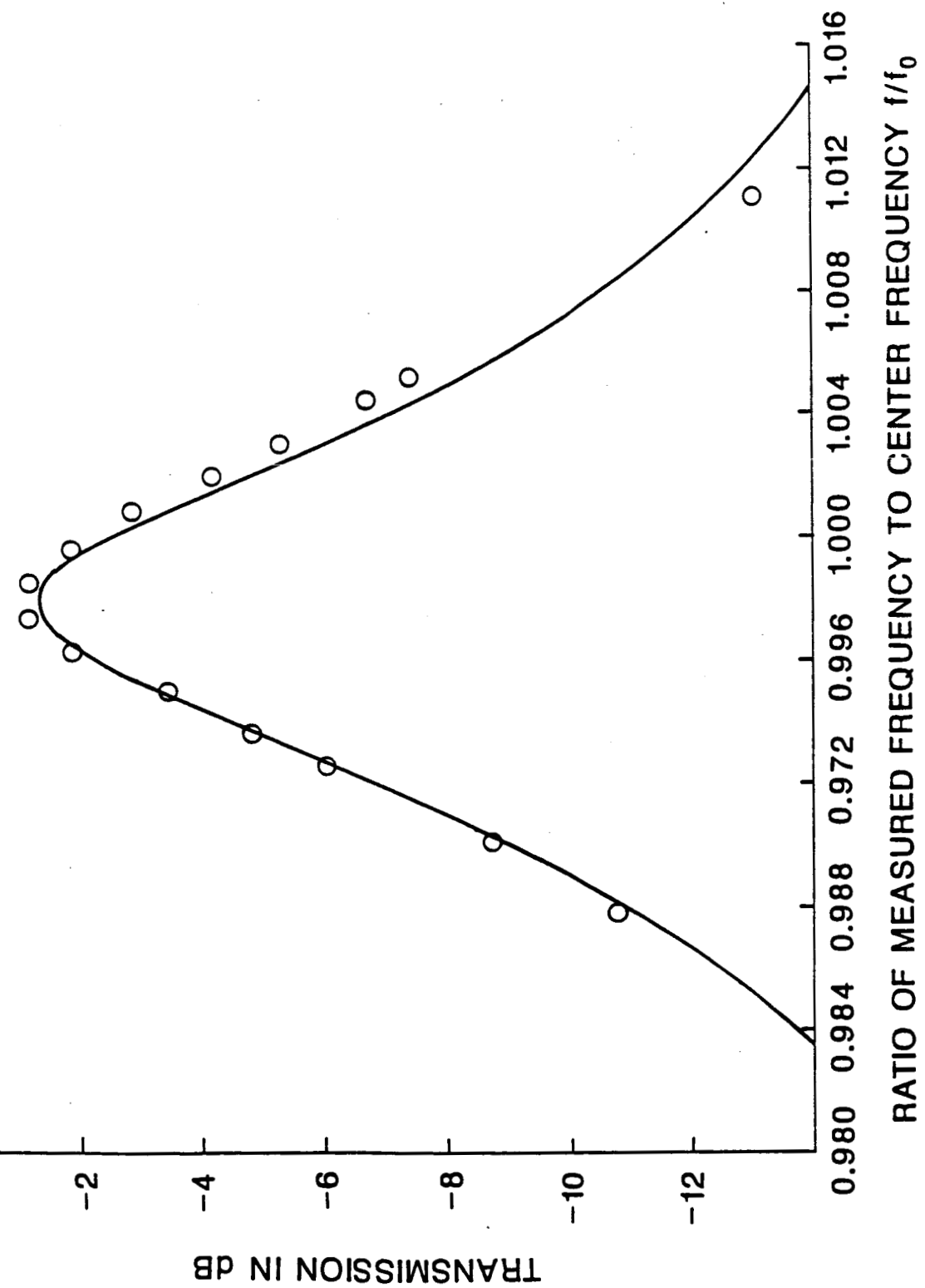


Figure 5-2. Comparison of calculated (solid line) and measured (circles) transmission of a four-grid array at 70 GHz. The angle between the grid wires was chosen to be  $85^\circ$ .

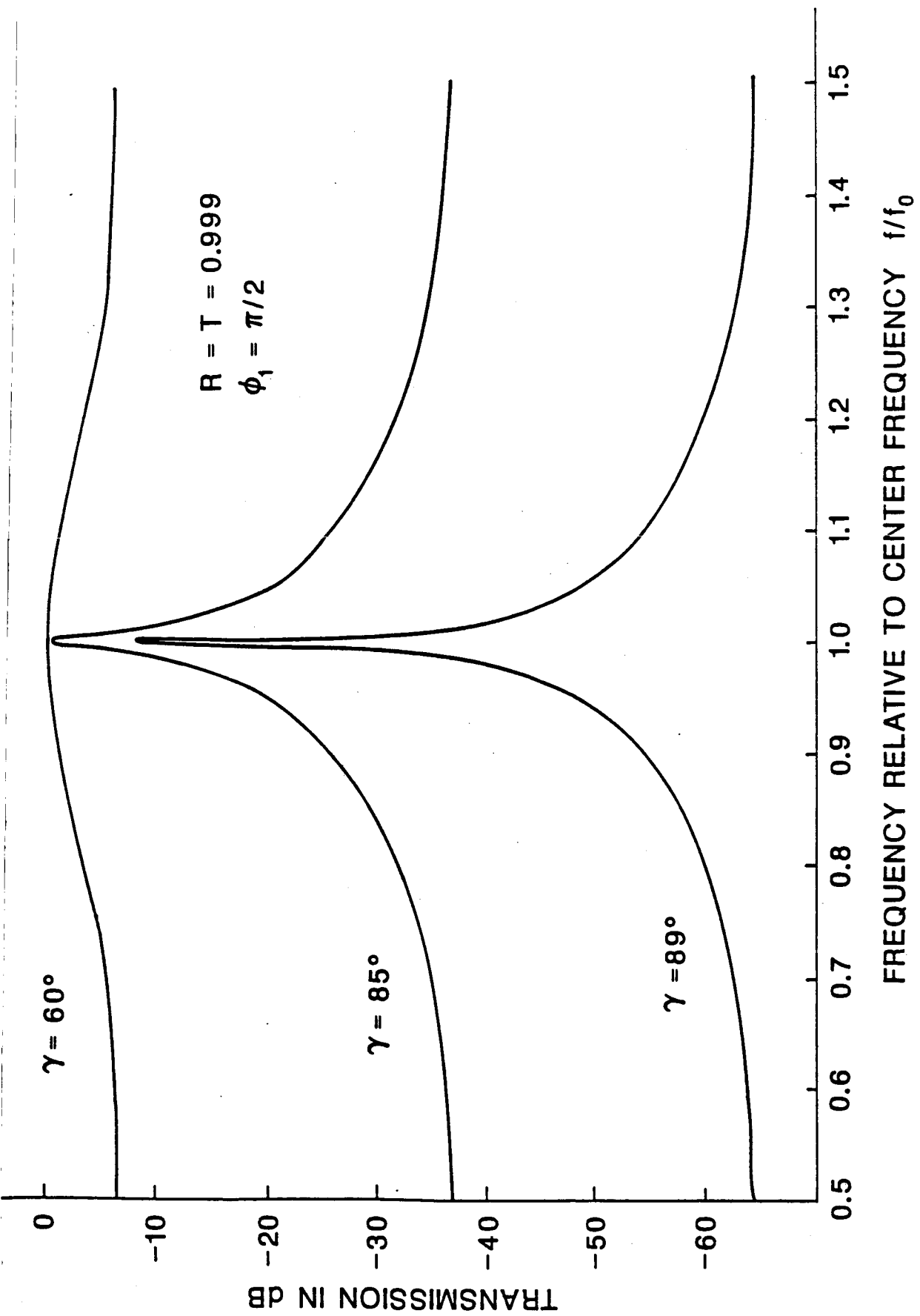


Figure 5-3. Calculated values of four-grid array transmission as a function of frequency for three different angles between grid pairs.

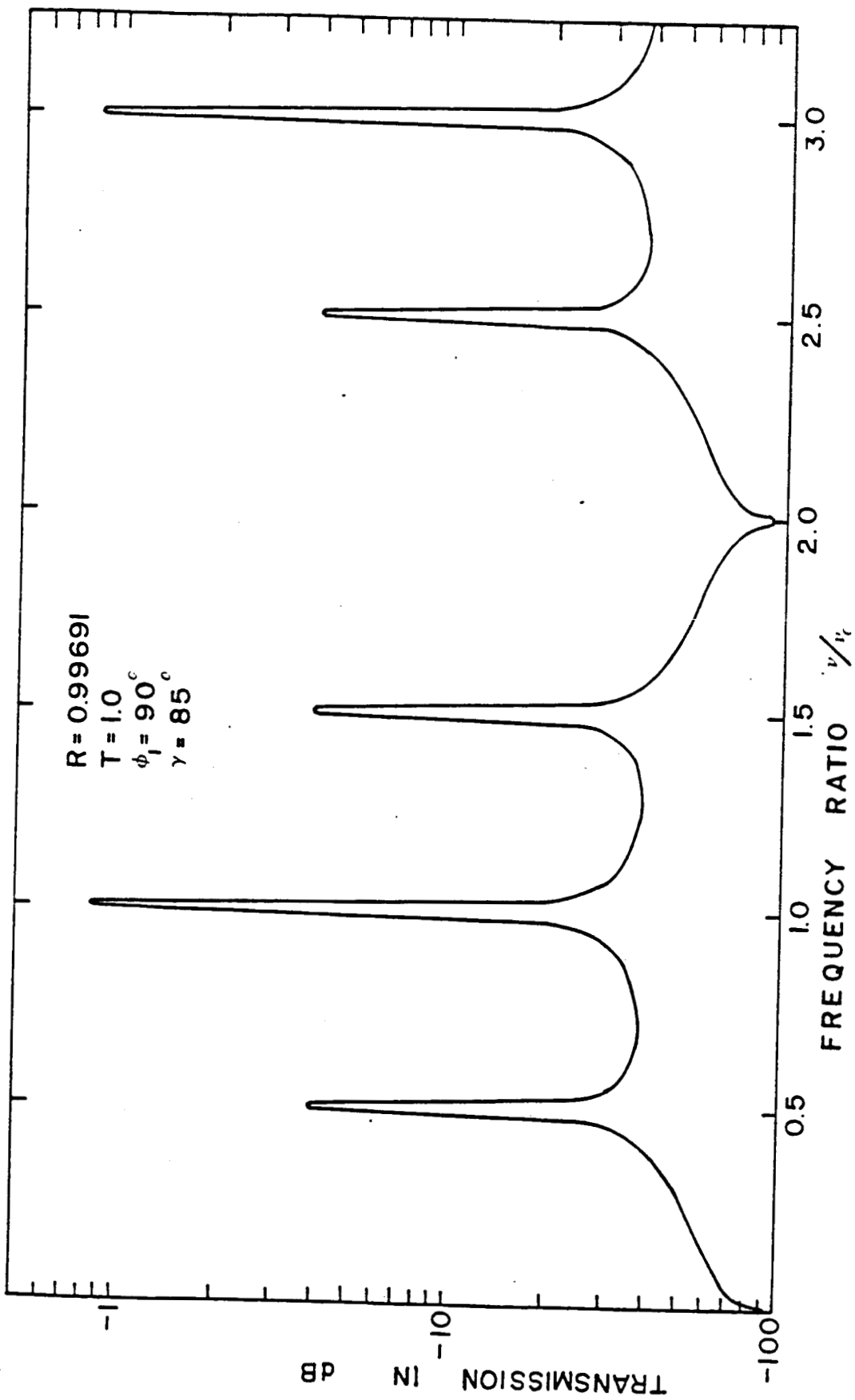


Figure 5-4. Four-grid array transmission vs. frequency, showing bandpass and band reject frequencies.

of wire grid arrays is that they are bandpass tunable, either by varying the angle between the grid pairs forming the interferometer, or by varying the spacing between elements of these pairs. Figure 5-3 shows calculated values of transmission as a function of displacement from the center frequency for several different values of the angle between grid pairs. Two features are immediately evident: (1) the transmission bandpass is indeed tunable by varying this angle, and (2) the peak transmission drops rapidly as the bandwidth is narrowed. This latter feature is also a property of optical interferometers, and results simply from the fact that interferometers with higher reflectivity plates will have greater loss because a larger number of internal reflections occur within the device.

One of the most interesting analytical results obtained for these grid arrays, not verified experimentally, is the prediction of both bandpass and band-reject capabilities. Figure 5-4 shows calculated transmission as a function of frequency for the center frequency of the interferometer, it is seen to behave as a bandpass filter, while for even multiples, the frequency is rejected to about 90 dB as shown. For frequencies between these values, the peak transmission is about -5dB. Note that for a conventional Fabry-Perot interferometer, a transmission peak would occur on each of the features of Figure 5-4. These results were obtained subject to the restriction that the properties of the grids, in particular reflection and transmission, remain constant over the range of frequencies over which the calculations were made.

To summarize this section, it appears that wire grid arrays have the potential for performing some very useful and interesting functions as quasi-optical MMW and sub-MMW devices, but this potential has been largely untapped. This potential is especially great for the higher frequencies and for radio astronomy applications, and may hopefully be soon realized with improved methods of grid fabrication and a greater awareness of

the capabilities of these devices.

## 6.0 Summary and Conclusions

During the period 1974-1986, the Georgia Tech Research Institute was supported by NASA grant NSG-5012 to perform research in millimeter wave techniques. This effort covered all areas of MMW research, but emphasis was placed on studies of atmospheric propagation, quasi-optical device development, and the development of MMW mixers. This report summarizes the work performed in each of these areas, but the amount of detail given is necessarily limited. For more detail on specific studies, the reader is referred to the series of semi-annual status reports published during the term of this grant, or to the numerous publications in the open literature supported by it.

Work in atmospheric propagation included both measurements and calculations of atmospheric attenuation and radiometric antenna temperatures under various atmospheric conditions. The profile of the water vapor absorption near 183 GHz was essentially verified, and the prediction of a sharp peak in temperature, which should be observed in downlooking radiometry, was made. Broadband calculations of atmospheric transmission and antenna temperatures were also made.

The mixer development portion of this grant was perhaps the most important from the point of view of overall contributions to MMW technology. The development of the f/2 and f/4 subharmonic mixer used for the airborne radiometers flown on the Convair 990 was perhaps the most important of these mixer contributions, since state-of-the-art noise performance was achieved with the great advantage of subharmonic operation. This mixer development also benefits the programs of other sponsors at Georgia Tech, in particular the U. S. Army Night Vision and Electro-Optics Laboratory, since an f/4 mixer was used in a system delivered to that agency. This mixer research continues to be a benefit; a 340 GHz f/4 subharmonic mixer is currently being developed for an

Army Missile Command program.

Research on MMW and sub-MMW components was also conducted, with emphasis on the development of quasi-optical techniques and devices and the fabrication of corrugated feed horns. Of particular interest was the derivation of equations for the transmission and reflection properties of wire grid arrays which give good agreement with experiment and predict some unusual properties for these devices, including bandpass tunability and filter characteristics which show both bandpass and band-reject capabilities. With improved fabrication techniques, excellent wire grids are becoming more readily available, and are expected to be used more frequently in the future, especially in the higher frequency systems and perhaps in specialized applications such as in radio astronomy.

This grant has also contributed to MMW technology in some areas not greatly emphasized in this report; for example in the fabrication of corrugated horn antennas, development of lenses made of plastic and matching of these devices, and the design and fabrication of MMW radiometer loads. This grant has provided the means for developing technology which has greatly benefited Georgia Tech, and it is hoped that benefits have also accrued to NASA and to the rest of the MMW community as well. Georgia Tech in general, and the personnel who have worked on this grant in particular, are very grateful to NASA for providing the long-term support which has enabled them to contribute to MMW technology, and to realize the personal satisfaction that results from making such contributions.

#### ACKNOWLEDGEMENTS

The author of this report is happy to acknowledge the support of numerous individuals, both at Georgia Tech and at NASA Goddard, who have contributed to the results obtained with support from this grant. In particular, the contributions and foresight of the late Mr. J. Larry King are very much appreciated, and the positive influences of his tenure as NASA technical monitor are evident in all areas of MMW research carried out with grant support. The other NASA technical monitors, W. T. Walton and L. R. Dod, have also contributed greatly to the success of this effort, and we at Georgia Tech are grateful for their help and insight. J. W. Dees was Georgia Tech project director during the early days of this program, and his energy and insight, together with his positive interactions with Larry King, did much to determine the course of this grant and the nature of its contributions. Mr. R. E. Forsythe was project director toward the end of this effort, and made significant contributions to MMW mixer technology with grant support. Finally, the great contributions of the many Georgia Tech students, secretaries, machinists, draftspersons, and professional staff, who worked on this grant, and are too numerous to name here, are gratefully acknowledged.

## REFERENCES

1. J. H. Van Vleck and V. F. Weisskopf, "On the Shape of Collision-Broadened Lines," Rev. Mod Phys., vol 17, pp. 227-236, Apr-July 1945.
2. G. W. King, R. M. Hainer, and P. C. Cross, "Expected Microwave Absorption Coefficients of Water and Related Molecules," Phys. Rev., vol. 71, pp. 433-443, Apr. 1947.
3. J. H. Van Vleck, "The Absorption of Microwaves by Uncondensed Water Vapor," Phys. Rev., vol. 71, pp. 425-433, Apr. 1947.
4. C. H. Townes and A. L. Schawlow, Microwave Spectroscopy. New York: McGraw-Hill, 1955, p. 104.
5. E. P. Gross, "Shape of Collision-Broadened Spectral Lines," Phys. Rev., vol. 97, pp. 395-403, Jan. 1955.
6. A. E. Schulze and C. W. Tolbert, "Shape, Intensity, and Pressure Broadening of the 2.53-Millimeter Wave-Length Oxygen Absorption Line," Nature, vol. 200, no. 4908, pp. 747-750, Nov. 23, 1963.
7. N. E. Gaut and E. C. Reifenstein III, Environmental Research and Technology Rep. No. 13, NASA Contract NAS8-26275, Waltham, MA, Feb. 1971.
8. G. T. Wrixon and R. W. McMillan, "Measurements of Earth-Space Attenuation at 230 GHz," IEEE Trans. Microwave Theory Tech., vol. MTT-26, No. 6, June 1978, pp. 434-439.

9. D. L. Croom, "Stratospheric Thermal Emission and Absorption Near the 22.235 Gc/s (1.35 cm) Rotational Line of Water-Vapor," *J. Atmos. Terr. Phys.*, vol. 27, pp. 217-233, 1965.
10. --, "Stratospheric thermal emission and absorption near the 183.311 Gc/s (1.64 mm) rotational line of water-vapor," *J. Atmos. Terr. Phys.*, vol 27, pp. 235-243, 1965.
11. A. H. Barrett and V. K. Chung, "A Method for the Determination of High-Altitude Water-Vapor Abundance from Ground-Based Microwave Observations," *J. Geophys. Res.*, vol. 67, pp. 4259-4266, Oct. 1962.
12. H. J. Liebe and D. H. Layton, "Near-Millimeter-Wave Attenuation and Delay Rates by Moist Air," Proc. 1987 International Geoscience and Remote Sensing Symposium, University of Michigan, Ann Arbor, May 1987.
13. G. G. Gimmesstad and H. A. Gebbie, "Atmospheric absorption in the range  $12 \text{ cm}^{-1}$  to  $32 \text{ cm}^{-1}$  measured in a horizontal path," *J. Atmos. Terr. Phys.*, vol. 38, pp. 325-328, 1976.
14. H. R. Carlon, "Infrared Water Vapor Continuum Absorption: Equilibria of Ions and Neutral Water Clusters," *Appl. Opt.*, vol. 20, No. 8, 15 April 1981, pp. 1316-1322.
15. R. W. McMillan, J. J. Gallagher and A. M. Cook, "Calculations of Antenna Temperature, Horizontal Path Attenuation, and Zenith Attenuation Due to Water Vapor in the Frequency Band 150-700 GHz," *IEEE Trans. Microwave Theory Tech.*, vol. MTT-25, No. 6, June 1977, pp. 484-488.

16. J. J. Gallagher and R. W. McMillan, "Prediction of the Existence of a Sharp Peak in Water Vapor Emission Lines in Down-Looking Radiometry," Third International Conference on Infrared and Millimeter Waves, University of Surrey, Guilford, England, March 1978.
17. J. Gustincic, Private Communication, January 1976.
18. R. E. Forsythe, V. T. Brady, and G. T. Wrixon, "Development of a 183 GHz Subharmonic Mixer," Proc. 1979 IEEE-MTT Symposium, Orlando, Florida, April/May 1979.
19. M. Born and E. Wolf, Principles of Optics, Pergamon Press, New York, (1965), pp. 323-333.
20. R. W. McMillan, "Transmission Properties of Four-Grid Arrays," Fifth International Conference on Infrared and Millimeter Waves, University of Wurzburg, Wurzburg, Germany, October 1980.